# A review of polymer dissolution

## Beth A. Miller-Chou, Jack L. Koenig*

*Department of Macromolecular Science, Case School Engineering, Case Western Reserve University, 10900 Euclid Avenue, Cleveland, OH 44106, USA*

## Abstract

Polymer dissolution in solvents is an important area of interest in polymer science and engineering because of its many applications in industry such as microlithography, membrane science, plastics recycling, and drug delivery. Unlike non-polymeric materials, polymers do not dissolve instantaneously, and the dissolution is controlled by either the disentanglement of the polymer chains or by the diffusion of the chains through a boundary layer adjacent to the polymer–solvent interface. This review provides a general overview of several aspects of the dissolution of amorphous polymers and is divided into four sections which highlight (1) experimentally observed dissolution phenomena and mechanisms reported to this date, (2) solubility behavior of polymers and their solvents, (3) models used to interpret and understand polymer dissolution, and (4) techniques used to characterize the dissolution process.
© 2003 Elsevier Ltd. All rights reserved.

*Keywords:* Amorphous polymers; Diffusion; Dissolution; Dissolution models; Dissolution mechanisms; Permeation; Polymer; Review; Solubility; Solvents; Swelling

## Contents

* Corresponding author. Tel.: +1-216-368-4176; fax: +1-216-368-4171.
  *E-mail address:* jlk6@po.cwru.edu (J.L. Koenig).

# 1. Introduction

Polymer dissolution plays a key role in many industrial applications in a variety of areas, and an understanding of the dissolution process allows for the optimization of design and processing conditions, as well as selection of a suitable solvent. For example, microlithography is a process used to fabricate microchips. Generally, this process consists of five steps [1]. First, a photosensitive polymer or photoresist solution is spin coated onto a substrate surface, usually silicon or gallium arsenide, where it forms a very thin film. Second, a mask with the desired pattern is placed over the polymer, and then the resist is exposed to electromagnetic irradiation. The type of radiation chosen depends on the polymer system and

produces the desired physical and/or chemical changes in the polymer resist. If the exposed portions of the polymer film degrade and become more soluble, a positive resist is formed. However, if the exposed polymer regions are crosslinked, rendering these resists less soluble in the developer solvent, a negative resist is formed. Next, the pattern formed by the radiation on the resist is developed by treatment with solvents that remove either the irradiated (positive resist) or the non-irradiated regions (negative resists). The resulting polymeric image of the mask pattern is then transferred directly onto the substrate by wet or plasma etching. Once the desired pattern is on the substrate, the remaining polymer resist is stripped off the substrate. The resolution of the final pattern image is crucial for integrated

# Nomenclature

| | |
|---|---|
| $M_N$ | number average molecular weight |
| $M_W$ | weight average molecular weight |
| $\chi_{AB}$ | Flory–Huggins interaction parameter |
| $V_{ref}$ | reference volume |
| $\delta_i$ | solubility parameter of species $i$ |
| $R$ | gas constant |
| $T$ | absolute temperature |
| $\Delta G_m$ | Gibbs free energy change on mixing |
| $\Delta H_m$ | enthalpy change on mixing |
| $\Delta S_m$ | entropy change on mixing |
| $V_{mix}$ | volume of the mixture |
| $\Delta E_i^V$ | energy of vaporization of species $i$ |
| $V_i$ | molar volume of species $i$ |
| $\Phi_i$ | volume fraction of $i$ in the mixture |
| CED | cohesive energy density |
| $\Delta H_{vap}$ | enthalpy of vaporization |
| $E$ | cohesive energy |
| $T_c$ | critical temperature |
| $T_b$ | normal boiling temperature |
| $\sum \Delta_T$ | Lyderson constant |
| $\varepsilon$ | dielectric constant |
| $n_l$ | refractive index of the liquid |
| $\mu$ | dipole moment (Debye) |
| $\Delta h_i$ | contribution of the $i$th atom or group to the molar heat of vaporization |
| $U$ | internal energy |
| $F$ | molar attractive constant |
| $P$ | pressure |
| $V_g$ | specific volume of the gas phase |
| $V_l$ | specific volume of the liquid phase |
| $M$ | molecular weight |
| $P_c$ | critical pressure |
| $\rho$ | density |
| $\Delta H_{vap}^0$ | heat of vaporization at some standard temperature |
| $\Delta e_i$ | additive atomic contributions for the energy of vaporization |
| $\Delta v_i$ | additive group contributions for the energy of vaporization |
| $n$ | number of main chain skeletal atoms |
| $X$ | degree of crystallization |
| $V_c$ | molar volume crystalline phase |
| $\chi$ | Flory–Huggins chi parameter |
| $\chi_{sp}$ | solvent–polymer interaction parameter |
| $a$ | entropic part of $\chi$ |

| | |
|---|---|
| $b$ | enthalpic part of $\chi$ |
| $R_o$ | radius of the Hansen solubility sphere |
| $R_a$ | solubility parameter distance |
| RED | relative energy density |
| $f$ | Teas fractional parameters |
| $l$ | initial half thickness of a polymer slab |
| R | polymer–gel interface position |
| S | solvent–gel interface position |
| $j_s$ | solvent diffusional flux |
| $D_s$ | diffusion coefficient of the solvent |
| $F$ | function |
| $x$ | distance |
| $t$ | time |
| $v_s$ | swelling velocity |
| $R_d$ | disassociation/dissolution rate |
| $D_p$ | diffusion coefficient of the polymer |
| $L$ | external polymer thickness |
| $t_{rep}$ | reptation time |
| $k_i$ | mass transfer coefficient of species $i$ |
| $r$ | radial position |
| $r_0$ | initial radius of the polymeric particle |
| $\phi_{s,eq}$ | equilibrium volume fraction of the solvent in the polymer |
| $\phi_{p,eq}$ | equilibrium volume fraction of the polymer in the solvent |
| $k_d$ | disengagement rate |
| $\phi_{p,b}$ | polymer volume fraction in the bulk |
| $Pe_R$ | Peclet number |
| $D_{ig}$ | dimensionless diffusivities of species $i$ in the gel phase |
| $k_{eff}$ | effective disengagement rate |
| $\alpha$ | ratio of the reference length scale to the product of the reference time and the reference velocity scales |
| $v_r$ | $r$-component of the velocity |
| $v_\theta$ | $\theta$-component of the velocity |
| $S_\phi$ | source term |
| $v_{sp}$ | velocity of the gel–solvent interface |
| $v_{s\infty}$ | external velocity |
| $K$ | parameter of kinetic model for glass transition, Eq. (68) |
| $n$ | parameter of kinetic model for glass transition, Eq. (68) |
| $\phi_{s\|x=R}$ | concentration of the solvent at the interface of the swollen and glassy polymer |

| | |
|---|---|
| $\phi_{s,t}$ | concentration level corresponding to the threshold activity for swelling |
| $m_p$ | mobility of polymer chains |
| $m_{p,\infty}$ | maximum mobility that the polymer molecules can attain at infinite time under a state of maximum possible disentanglement at that concentration |
| $B_d$ | parameter which depends on the size of the mobile species |
| $f_{gp}$ | free volume fraction of the gel phase |
| $f_{pp}$ | free volume fraction of the polymer phase |
| $f_{sp}$ | free volume fraction of the solvent phase |
| $N_e$ | time dependent number of moles of physical entanglements |
| $N_{e,\infty}$ | number of moles of entanglement at large time corresponding to the concentrated polymer solution at that concentration |
| $M_c$ | critical molecular weight for entanglement of a polymer |
| $k_{diss}$ | dissolution rate constant |
| $M_{pt}$ | dry matrix mass at time $t$ |
| $m_{p0}$ | dry matrix mass at $t = 0$ |
| $A$ | surface area of the system at time $t$ |
| $D_s^v$ | volume-based diffusion coefficient of the solvent |
| $\phi_s^*$ | solvent volume fraction at which the glassy–gel transition occurred |
| $\delta$ | gel layer thickness |
| $\phi_{p,eq}^*$ | equilibrium polymer volume fraction at the front $S$ |
| $c_i$ | concentration of species $i$ |
| $\sigma$ | network stress |
| $\pi$ | osmotic pressure |
| $l$ | characteristic length Eq. (93) |
| $\mu_i$ | chemical potential of the species $i$ |
| $V_{a,i}$ | average volume of molecule of species $i$ |
| $Z$ | number of segments in the primitive path |
| $\Delta G_{seg}^{OR}$ | orientational contribution to the free energy |
| $k_B$ | Boltmann's constant |
| $B$ | parameter Eq. (96) |
| $\Phi$ | factor that determines the extent of the local swelling Eq. (97) |
| $l_m$ | monomer length |
| $r_g$ | radius of gyration |
| $D_{self}$ | self-diffusion coefficient |
| $C$ | empirical constant Eq. (104) |
| $\sigma_c$ | critical stress for crazing |
| $\gamma$ | constant Eq. (106) |
| $T_g$ | glass transition temperature |
| $\xi$ | distance between entanglements |
| $g$ | number of monomer units in an entanglement subunit |
| $\eta i$ | viscosity of species $i$ |
| $t_d$ | disentanglement time |
| $v^\dagger$ | $x$-component of the volume average velocity |
| $D$ | mutual diffusion coefficient |
| $C_p$ | dimensionless polymer concentration |
| $\tau$ | dimensionless time |
| $\lambda$ | dimensionless length scale |
| $\kappa$ | exponential parameter Eq. (123) |
| $r$ | ratio for concentration dependence Eq. (124) |
| $\phi_{s,c}$ | critical solvent concentration |
| $D_{s,0}$ | diffusivity of the solvent in a glassy polymer |
| $v_s$ | convective velocity of the solvent in the $x$-direction |
| $V_{s,s}$ | specific volume of the solvent |
| $\sigma_{xx}$ | normal stress |
| $E$ | spring modulus |
| $M_d$ | mass of drug |
| $\phi_{ic}$ | characteristic concentrations of species $i$ |
| $\phi_{d,eq}$ | equilibrium concentration of the drug |
| $\rho_{p,dis}$ | polymer disentanglement concentration |
| $D_{eff}$ | effective diffusion coefficient |
| $D_{Zimm}$ | Zimm diffusion coefficient |
| $E_i$ | electric field amplitude of incident light |
| $E_r$ | electric field amplitude of reflected light |
| $r_c^{\parallel}$ | parallel reflection coefficient |
| $r_c^{\perp}$ | perpendicular reflection coefficient |
| $\rho$ | ratio of parallel and reflection coefficients |
| $\Delta$ | parameter of Eq. (150) |
| $\psi$ | parameter of Eq. (150) |
| $T_1$ | spin–lattice |
| $T_2$ | spin–spin relaxation |

circuits. Therefore, minimal swelling and no cracking are desired. Other important features for a polymer to be useful in these applications are good adhesion to the substrate material, high photosensitivity, high contrast, chemical and physical resistance against the etchant, and easy stripping off the substrate [1]. It is worthy to note another electronic application where polymer dissolution is important is within the semiconductor industry. Because of their non-swelling nature, aqueous-base developability, and etching resistance, novolak dissolution has become an important process in these applications.

Another example where polymer dissolution becomes important is in membrane science, specifically for a technique, called phase inversion, to form asymmetric membranes. In this process, a polymer solution thin film is cast onto a suitable substrate followed by immersion in a coagulation bath (quench step) [2–5] where solvent/non-solvent exchange and eventual polymer precipitation occur. The final structure of the membrane is determined by the extent of polymer dissolution. Membranes used for microfiltration can be made by exposing a uniform film of crystallizable polymer to an alpha particle beam, causing it to become porous, and the crystalline structure is disrupted. The film is then chemically treated with an etchant, and nearly cylindrical pores are produced with a uniform radius. Another way to produce a microfiltration membrane is to cast films from pairs of compatible, non-complexing polymers. When the films are exposed to a solvent which only dissolves one of the polymers, interconnected microvoids are left behind in the other polymer.

Polymer dissolution also plays an instrumental role in recycling plastics. A single solvent can be used to dissolve several unsorted polymers at different temperatures [6–8]. This process involves starting with a physical mixture of different polymers, usually packaging materials, followed by dissolution of one of the polymers in the solvent at a low temperature. This yields both a solid phase containing polymers which are insoluble in the solvent (at the initial temperature) and a solution phase. The solution phase containing the polymer which dissolved at the low temperature is then drained to separate parts of the system, eventually vaporizing the solvent, leaving behind pure polymer. The solvent is then sent back to the remaining solid phase where it is heated to a higher temperature, another polymer dissolves, and the process is repeated. Several of these cycles are performed at increasing temperatures until almost all pure, separate polymers are obtained [2].

Within the field of controlled drug delivery and time-released applications, knowledge of polymer dissolution behavior can be vital. An ideal drug delivery system is one which provides the drug only when and where it is needed, and in the minimum dose level required to elicit the desired therapeutic effects [9]. Within these systems a solute/drug is dispersed within a polymer matrix. When the system is introduced to a good solvent for the polymer, swelling occurs allowing increased mobility of the solute, and it diffuses out of the polymer into the surrounding fluid. Such a system should provide a programmable concentration–time profile that produces optimum therapeutic responses. Recent developments in polymeric delivery systems for the controlled release of therapeutic agents has demonstrated that these systems not only can improve drug stability both in vitro and in vivo by protecting unstable drugs from harmful conditions in the body, but also can increase residence time at the application site and enhance the activity duration of short half-life drugs. Therefore, compounds which otherwise would have to be discarded due to stability and bioavailability problems may be rendered useful through a proper choice of polymeric delivery system [9].

Polymer dissolution is also being currently investigated for tissue regeneration [10,11]. Many strategies in this field depend on the manipulation of polymers which are suitable substrates for cell culture and implantation. Using computer-aided design and manufacturing methods, researchers will shape polymers into intricate scaffolding beds that mimic the structure of specific tissues and even organs. The scaffolds will be treated with compounds that help cells adhere and multiply, then 'seeded' with cells. As the cells divide and assemble, the polymer dissolves away. The new tissue or organ is then implanted into the patient. During the past several years, human skin grown on polymer substrates has been grafted onto burn patients and foot ulcers of diabetic patients, with some success. Structural tissues, ranging from urethral tubes to breast tissue, can be fabricated according to the same principle. After mastectomy, cells that are grown on biodegradable polymers would

be able to provide a completely natural replacement for the breast. Degradable polymers may be useful in orthopedic applications because they circumvent the problems of a persistent foreign body and the need for implant retrieval [11]. However, most of these polymers are not mechanically strong enough to be used for load bearing applications.

As one can see, polymer dissolution proves to be very important to several applications such as microlithography, membrane science, plastics recycling, and drug delivery. Newer applications such as tissue engineering are also of current investigation. A thorough understanding of the polymer dissolution process and mechanism enables improvement and optimization of fabrication conditions and desired final physical properties.

## 2. Polymer dissolution behavior

Polymer dissolution has been of interest for some time and some general behaviors have been characterized and understood throughout the years. The dissolution of non-polymeric materials is different from polymers because they dissolve instantaneously, and the dissolution process is generally controlled by the external mass transfer resistance through a liquid layer adjacent to the solid–liquid interface. However, the situation is quite diverse for polymers. The dissolution of a polymer into a solvent involves two transport processes, namely solvent diffusion and chain disentanglement. When an uncrosslinked, amorphous, glassy polymer is in contact with a thermodynamically compatible solvent, the solvent will diffuse into the polymer (Fig. 1). Due to plasticization of the polymer by the solvent, a gel-like swollen layer is formed along with two separate interfaces, one between the glassy polymer and gel layer and the other between the gel layer and the solvent. After time has passed, an induction time, the polymer dissolves. However, there also exist cases where a polymer cracks and no gel layer is formed.

The following section summarizes important results of various experimental studies that have contributed to the understanding of polymer dissolution mechanisms and behavior of amorphous
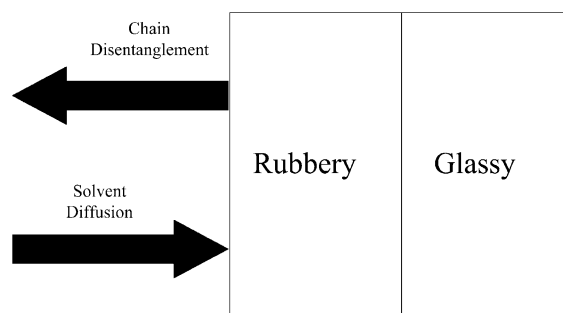


Fig. 1. A schematic of one-dimensional solvent diffusion and polymer dissolution. (Adapted from Ref. [2].)

glassy systems, but some crosslinked systems are discussed.

### 2.1. Surface layer formation and mechanisms of dissolution

One of the earliest contributors to the study of polymer dissolution was Ueberreiter [12] who outlined the surface layer formation process. First, the solvent begins its aggression by pushing the swollen polymer substance into the solvent, and, as time progresses, a more dilute upper layer is pushed in the direction of the solvent stream. Further penetration of the solvent into the solid polymer increases the swollen surface layer until, at the end of the swelling time, a quasistationary state is reached where the transport of the macromolecules from the surface into the solution prevents a further increase of the layer.

Ueberreiter went on to summarize the structure of the surface layers of glassy polymers during dissolution from the pure polymer to the pure solvent as follows: the infiltration layer, the solid swollen layer, the gel layer, and the liquid layer (Fig. 2). The infiltration layer is the first layer adjacent to the pure polymer. A polymer in the glassy state contains free volume in the form of a number of channels and holes of molecular dimensions, and the first penetrating solvent molecules fill these empty spaces and start the diffusion process without any necessity for creating
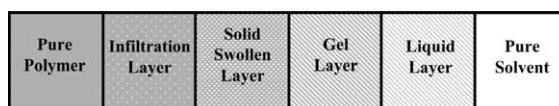


Fig. 2. Schematic picture of the composition of the surface layer.

new holes. The next layer is the solid swollen layer where the polymer–solvent system building up in this layer is still in the glassy state. Next, the solid swollen layer is followed by the gel layer, which contains swollen polymer material in a rubber-like state, and a liquid layer, which surrounds every solid in a streaming liquid, respectively.

Two types/mechanisms of dissolution were proposed. With the first type of dissolution, termed 'normal dissolution', all the layers described above are formed. The second type of dissolution occurs when no gel layer is observed. In a study by Asmussen and Raptis [13], poly(methyl methacrylate) (PMMA) was dissolved in several solvents and showed the normal dissolution process beginning at the glass transition temperature. By decreasing the experimental temperature, a steady decrease in the gel layer thickness could be seen until finally a temperature was reached where this part of the total surface layer was so thin that it was no longer visible. Below this temperature, cracks were observed running into the polymer matrix, and these cracks coalesced and caused small blocks of the polymer to leave the surface in a kind of eruption process. The reason for the cracking mechanism was proposed to be the freezing-in of large amounts of stress energy in the polymer in the glass transition interval. The gel temperature (where the transition from normal dissolution to cracking) was formally defined as the temperature at which the gel layer disappeared. Conversely with other experiments with polystyrene (PS), Ueberreiter and Asmussen observed that PS underwent normal dissolution in most solvents owing to its low gel temperature [14].

Krasicky et al. [15,16] monitored the transition layer during the dissolution process and found that it increases with the molecular weight of the polymer. Also, when PMMA dissolved in methyl ethyl ketone (MEK), the transition layer was not detectable below a polymer number average molecular weight, $M_N$, of about 30 000. They concluded that the rate of the dissolution process is governed primarily by what is happening near the interface with the solid polymer, rather than by what is happening elsewhere in the transition layer.

Pekcan et al. [17] monitored the dissolution of annealed high-$T_g$ latex films in real time. They defined three stages of dissolution for these films. In the first

stage, swelling dominates and the gel layer thickness increases with time. This stage occurs within the first 60–100 s, depending on the annealing time of the film. At a later time, during stage two, there is a time period where the gel layer thickness remains constant due to swelling and dissolution. Finally, in the last stage, the gel layer thickness decreases with time due to desorption of polymer chains.

## 2.2. Effect of polymer molecular weight and polydispersity

In Ueberreiter's early research in polymer dissolution, several aspects were investigated, one of which was the polymer molecular weight effect on the dissolution [12]. It was found that the dissolution rate decreases with increased polymer molecular weight. Cooper et al. [18] also studied the effects of molecular weight on the dissolution rates of thin PMMA films, and found that dissolution results in a non-linear behavior when the log dissolution rate was plotted against the log $M_N$. Also, Manjkow et al. [19] discovered that dissolution not only can be affected by the polymer molecular weight, but also by its polydispersity. They found that polydisperse samples dissolved about twice as fast as monodisperse ones of the same $M_N$.

Papanu et al. [20] observed that the dissolution rate of PMMA with methyl isobutyl ketone (MIBK) is inversely proportional to the polymer molecular weight up to a molecular weight of 100 000 and then the rate levels off at higher molecular weights. Below this critical molecular weight, dissolution occurred by stress cracking, therefore, it was proposed that the critical stress for crazing was dependent on molecular weight of the polymer. In addition, the thickness of the gel layer was monitored for the ketone dissolutions, and when MIBK was used, a swollen surface layer formed during an initial induction period, and the thickness of the layer increased with polymer molecular weight. However, no swollen layer was seen below a polymer molecular weight of $10^5$ g/mol, which again indicated stress cracking. Later, the effect of polymer molecular weight on methanol (MeOH) penetration rates was investigated with monodisperse PMMA (21–27 °C), and a minimum rate occurred at an intermediate polymer molecular weight [21].

In another study, Parsonage et al. [22] concluded that the dissolution is controlled by chain disentanglement, which is a function of polymer molecular weight. Larger molecular weights yield higher levels of disentanglement. Therefore, these molecular weights have a higher degree of swelling before dissolution occurs.

Pekcan and co-workers [23,24] later researched the molecular weight and thickness effects on latex dissolution. They reported an inverse relationship between polymer desorption and weight average molecular weight, $M_W$. Also, thicker and opaque films dissolve much faster than the thinner and transparent films. This phenomenon is related to the pores and cracks created in thicker films during annealing. These imperfections increase the surface area in films against solvent molecules and as a result thicker films dissolved faster.

## 2.3. Effect of polymer structure, composition and conformation

Besides the molecular weight of the polymer, the dissolution process can also be affected by the chain chemistry, composition and stereochemistry. Ouano and Carothers [25] studied in situ dissolution dynamics of PS, poly($\alpha$-methyl styrene) (PAMS), and two tactic forms of PMMA. Similar to Ueberreiter's observations [12], they found that PS developed a thick swollen layer while PMMA cracked when exposed to the same solvent, MEK. They accounted for the differences in dissolution behavior to both the mass and momentum transports in the swelling polymer matrix. Thus, the polymer dissolves either by exhibiting a thick swollen layer or by undergoing extensive cracking, depending on how fast the osmotic pressure stress that builds up in the polymer matrix is relieved. Therefore, the nature of the polymers and differences in free volume and segmental stiffness are responsible for behavior variations from polymer to polymer. They also found that the dissolution behavior is profoundly affected by the tacticity of the polymer. Large cracks formed when atactic PMMA was dissolved in MIBK, but no cracks were seen in isotactic PMMA with the same solvent. This behavior correlates with the glass transition temperature ($T_g$) and the same phenomenon occurring as discussed above. Gipstein et al. [26] also observed

variations of dissolution behavior with stereochemistry in that the solubility rate of isotactic PMMA is much greater than that for the syndiotactic and heterotactic stereoforms.

Groele and Rodriguez [27] investigated the effect of polymer composition on the dissolution rate. They studied homopolymer of methyl methacrylate (MMA), ethyl methacrylate (EMA), *n*-butyl methacrylate (BMA) as well as copolymers of MMA with EMA and BMA. The polymer dissolution rate in MIBK at 30 °C varied from 0.042 $\mu$m/min (PMMA) to more than 150 $\mu$m/min (PBMA), showing that copolymers of MMA with EMA and BMA dissolve more rapidly than PMMA. They proposed that these observations were due to the thermodynamic compatibility of the copolymers with MIBK and the $T_g$ of the copolymers. Reinhardt et al. [28] also studied the dissolution of a PMMA copolymer, poly(methyl methacrylate-*co*-methacrylic acid). These particular copolymers are interesting because at moderate baking temperatures, they undergo an intramolecular cyclization producing terpolymers containing anhydride moieties. Therefore, the dissolution behavior is changed and ketone solubilities are enhanced. The copolymer was tested with MEK and mixtures of ethyl glycol (EG). The findings were in agreement with a relaxation-controlled dissolution behavior, especially for the anhydride-containing terpolymer. No residual layers or pronounced induction times indicative of formation of a gel layer was observed, but a normal dissolution process with a very small gel layer was suggested. Within the prebaking temperature range from 130 to 230 °C, the dissolution rates for both MEK and MEK/EG rose continuously, and the rates also increased when samples were exposed to prolonged baking times, reflecting the changes in polymer composition during thermal annealing in the solid layer.

## 2.4. Effects of different solvents and additives

The type of penetrating solvent can also have a profound affect on polymer dissolution. Ouano and Carothers [25] studied the dissolution of PMMA in several solvents including tetrahydrofuran (THF), methyl acetate (MA), and MIBK. Crack initiation occurred quicker with the smaller, better solvents MA and THF than with the more bulky and poorer solvent, MIBK, because of higher diffusion rates and swelling

power of these solvent molecules. They concluded that if the 'internal pressure' builds up faster than the glassy matrix can relax through gradual swelling, catastrophic fracture results. Also, they pointed out that polymer morphology at the molecular level has a strong influence on the kinematics of dissolution.

Ouano [29] investigated the effect of residual solvent content on the dissolution kinetics of polymers. In this study, the dissolution rate of PMMA, cresol-formaldehyde resin (novolac), and a mixture of novolac resin and adiazo-photoactive compound (PAC) showed interesting results. First, a few percent change in the solvent content meant several orders of magnitude change in solubility rate. Therefore, the dependence of the dissolution rate on the residual solvent content is very strong, and the dissolution rate-solvent content relationship can be interpreted in terms of the free volume theory. Second, addition of the PAC to the novolac resin decreased the residual solvent content of the resists at any prebaking temperature. For example, at 85 °C prebake, pure resin contained ca. 14% solvent, while the resist or the resist analog contained only ca. 9.5% by weight. Lastly, a very rapid drying of PMMA at 160 °C resulted in very fast dissolution rate. This rapid evolution of the solvent leaves 'extra free volume' and strain in the PMMA.

Cooper et al. [30] investigated PMMA dissolution rates with mixed solvents. It was found that the addition of small non-solvent molecules to a good solvent results in a significant increase in the dissolution rate of PMMA films. This enhancement of the rate was proposed to be the result of 'plasticization' of the polymer films by the small, rapidly diffusing non-solvent molecules. Those molecules found to exhibit this enhancement effect at lower concentrations were water, methanol, and ethanol. Higher alcohols only decreased the dissolution rate of the films. It was also noted that high concentrations of the non-solvent molecules caused the films to swell appreciably. In addition, this enhancement effect was found to be less significant in lower molecular weight PMMA when compared with higher molecular weights.

Mixed solvents were also studied by Manjkow et al. [31]. Solvent/non-solvent binary mixtures of MEK and isopropanol (MEK/IpOH) and MIBK and methanol (MIBK/MeOH) were used. A sharp transition

between complete solubility and almost total insolubility was observed in a narrow concentration range near 50:50 (by volume) solvent/non-solvent for both mixtures. In the insoluble regime, the polymer swelled up to three times its initial thickness. At 50:50 MEK/IPA, a temperature decrease from 24.8 to 18.4 °C caused a change from complete dissolution to combined swelling/dissolution behavior and rendered the PMMA film only 68% soluble. For MEK/IPA, penetration rates increased with increasing MEK concentration. However, for the MIBK/MeOH, a maximum rate occurred at 60:40 MIBK/MeOH.

Papanu et al. [20] studied the PMMA dissolution in ketones, binary ketone/alcohol mixtures and hydroxyketones. They found that the dissolution rate decreases with increasing solvent size, indicating that dissolution rate is limited by the rate of which solvent molecules penetrate. For binary mixtures of acetone/isopropanol, a transition from swelling to dissolution occurred near acetone volume fractions of 0.45–0.5. Acetol caused only swelling, whereas diacetone alcohol dissolved the films at approximately a quarter of the rate of MIBK. Later, the effects of solvent size were also investigated [21]. Penetration rates were strongly dependent on solvent molar volume for methanol, ethanol, and isopropoanol, but 1-butanol and 2-pentanol had rates similar to isopropanol. Some of the lower molecular weight films cracked in MeOH (relatively low temperatures), but with the same molecular weight samples, no cracking was observed with isopropanol (at elevated temperatures). Papanu et al. explained this phenomenon by the isopropanol molecules not penetrating as easily as the smaller MeOH molecules, and at higher temperatures, the polymer chains can relax more readily. Both of these factors inhibit the buildup of catastrophic stress levels, and cracking is suppressed at higher polymer molecular weights. Gipstein et al. [26] observed that in a homologous series of *n*-alkyl acetate developer solvents, the molecular size of the solvent has a greater effect on the solubility rate than the molecular weight of the resist.

Mao and Feng [32] studied the dissolution process of PS in concentrated cyclohexane, a theta solvent for PS. They proposed a two-step process for dissolution within this system. First, swelling of the polymer below the $\theta$ temperature corresponds to the gradual dispersion of the side-chain phenyl groups which

are solvated by cyclohexane molecules; while the complete dissolution above the $\theta$ temperature corresponds to the gradual dispersion of the main chains at a molecular level. These dispersions reflect the fact that cohesional interaction among side-chain-phenyl rings or main chains are weakened by solvent molecules, which shows the existence of the cohesional entanglements among polymer chains.

Rodriguez et al. [33] made several contributions to the study of polymers used as positive photoresists in microlithographic applications. The found that plasticization of PMMA by poly(ethylene oxide) (PEO) of molecular weight 4000 changed the dissolution rate in direct proportion to the amount of PEO added. With a weight fraction of 0.2 PEO, the dissolution rate was double that for PMMA alone.

Harland et al. [34] studied the swelling and dissolution of polymer for pharmaceutical and controlled release applications. They researched the swelling and dissolution behavior of a system containing a drug and polymer. The dissolution was characterized by two distinct fronts: one separating the solvent from the rubbery polymer and the second separating the rubbery region from the glassy polymer. The drug release had a $t^{0.5}$ dependence relation to a diffusional term and a $t^1$ relation to a dissolution term, and the drug release rate was independent of time when the two fronts' movements were synchronized.

## 2.5. Effect of environmental parameters and processing conditions

External parameters such as agitation and temperature as well as radiation exposure can influence the dissolution process. Ueberreiter [12] found that the velocity of dissolution increases with the agitation and stirring frequency of the solvent due to a decrease of the thickness of the surface layer, and the dissolution rate approaches a limiting value if the pressure of the solvent against the surface of the polymer is increased (at all temperatures). Pekcan et al. also studied the effects of agitation and found that with no agitation, the solvent molecules penetrate the polymer, and a gel layer forms. However, the gel layer decreases in magnitude with time due to desorption of the polymer chains. On the other hand, when agitation

is present, no gel layer is formed because it is stripped off rapidly by the stirring process. In the latter case, the sorption of solvent molecules is immediately followed by desorption of the polymer chains from the swollen gel layer.

Manjkow et al. [19] conducted an investigation of the influence of processing and molecular parameters on the dissolution of these PMMA films with MIBK. They discovered that dissolution rates are highly sensitive to the molecular weight distribution, softbake cooling cycle, and dissolution temperature. The apparent activation energy for the dissolution of PMMA varied from 25 to 43 kcal/mol depending upon softbake cooling rates and molecular weight distribution. The dissolution rate of air quenched, monodisperse samples was found to vary with the molecular weight to the power of $-0.98$, but for slowly cooled samples, this constant was 85% higher.

Rao et al. [35] studied the influence of the spatial distribution of sensitizer on the dissolution mechanism of diazonaphthoquinone resists. Their studies demonstrated that the physical distribution of the PAC in the diazonaphthoquinone resists plays a significant role in the dissolution behavior of the films. For example, as little as 30 Å of PAC preferentially placed at the surface of the film or embedded between two polymer layers could cause significant induction period in development.

Parsonage and co-workers [22,36] investigated the properties of positive resists, both PMMA and its copolymers, and the effects of irradiation on degradation and sensitivity. They found that irradiation led to a drastic decrease in the molecular weights of all the homo- and copolymers studied. Planar and radial dissolution studies were performed in pure MEK or ethanol at 26 °C with PMMA and poly(methyl methacrylate-*co*-maleic anhydride) P(MMA-*co*-MAH). It was observed that the process of dissolution is dependent on the structure of the polymer. The initial stages of the dissolution mechanism consisted entirely of the polymer swelling. Once the swelling reached a critical point, the dissolution occurred and the polymer chains disentangled from the bulk and dissolved away. At this time, the two boundaries (gel–liquid and polymer–gel) proceeded at the same velocity.

Drummond et al. [37] studied the effects of radiation. With samples of P(MMA-*co*-MAH) with

MEK, it was shown that the dissolution process is a function of radiation dose, and the process started with swelling of the glassy polymeric slab by water which was followed by chain disentanglement and dissolution. It was also observed that when the swelling rate was greater than the dissolution rate, the gel layer thickness increased linearly with the square root of time, and, conversely, if the dissolution rate was greater than the swelling rate, then the gel thickness decreased with time.

## 3. Polymer solubility and solubility parameters

Solubility parameters are often used in industry to predict compatibility of polymers, chemical resistance, swelling of cured elastomers by solvents, permeation rates of solvents, and even to characterize the surfaces of pigments, fibers, and fillers [38,39]. Moreover, the usefulness of polymers in many technological applications is critically dependent on the solubility parameter, $\delta$, as noted by Bicerano [40]. Some of these applications are listed below.

(1) The removal of unreacted monomers, process solvents, and other synthesis of processing by-products, can both enhance the performance of the polymer and overcome health-related or environment-related objections to the use of certain types of polymers.
(2) The Flory–Huggins solution theory uses $\delta$ to determine whether two polymers (A and B) will be miscible by Eq. (1)

$$\chi_{AB} = [V_{ref}(\delta_A - \delta_B)^2]/RT \qquad (1)$$

The Flory–Huggins interaction parameter $\chi_{AB}$ is a function of temperature ($T$), the mole fraction of each polymer, and the degree of polymerization. In this equation, $V_{ref}$ is an appropriately chosen 'reference volume', often taken to be $100 \, cm^3/mol$, and $R$ is the gas constant. The blend miscibility is assumed to decrease with increasing $\chi_{AB}$. If strong interactions, e.g. hydrogen bonds, are present between structural units on polymers A and B, more elaborate versions of the Flory–Huggins solution theory can be used [41].

(3) Environmental crazing and stress cracking are dependent upon the solution and the diffusion of environmental agents in the polymer, and thus upon $\delta$ [42,43]. These phenomena are important in determining the length of time that a polymer part can be useful for its application.
(4) In some applications, the interaction of the polymer with a specific 'solvent' and/or with certain molecules carried by that solvent is not a detrimental event, but an essential aspect of the performance of the polymer. Reverse osmosis membranes and swollen hydrogels used in applications such as the desalination of water, kidney dialysis, soft contact lenses and surgical implants [44] are among such polymers.
(5) Plasticization is another area where the nature of the interaction of a polymer with molecules is critical to the usefulness of the polymer in many applications. Sears and Darby [45] have reviewed the importance of $\delta$ in the role of polymer-plasticizer compatibility for effective plasticization.

The solubility parameter is important in the theory of solutions and has been shown to be connected to other physical properties such as surface tension [46] and wettability [47–49], the ratio of the coefficient of thermal expansion to compressibility [50], the boiling points in the case of non-polar liquids [50], the ultimate strength of materials [51], and the glass transition temperature of polymers [52]. Therefore, the ability to estimate the solubility parameters can often be a useful tool to predicting systems' physical properties and performance.

It is the goal of this section to discuss the basis for solubility parameters, their use in predicting polymer dissolution, and the methods from which one can obtain the solubility parameters for both polymers (solute) and solvents.

### 3.1. Thermodynamics background

The solubility of a given polymer in various solvents is largely determined by its chemical structure. Polymers will dissolve in solvents whose solubility parameters are not too different from their

own. This principle has become known as 'like dissolves like', and, as a general rule, structural similarity favors solubility.

Dissolution of an amorphous polymer in a solvent is governed by the free energy of mixing [39]

$$\Delta G_m = \Delta H_m - T\Delta S_m \qquad (2)$$

where $\Delta G_m$ is the Gibbs free energy change on mixing, $\Delta H_m$ is the enthalpy change on mixing, $T$ is the absolute temperature, and $\Delta S_m$ is the entropy change on mixing. A negative value of the free energy change on mixing means that the mixing process will occur spontaneously. Otherwise, two or more phases result from the mixing process. Since the dissolution of a high molecular weight polymer is always associated with a very small positive entropy change, the enthalpy term is the crucial factor in determining the sign of the Gibbs free energy change. Solubility parameters were developed to describe the enthalpy of mixing [39].

Hildebrand pointed out that the order of solubility of a given solute in a series of solvents is determined by the internal pressures of the solvents [53]. Later, Scatchard introduced the concept of 'cohesive energy density' into Hildebrand's theories [54]. Hildebrand and Scott [50] and Scatchard [55] proposed that the enthalpy of mixing is given by

$$\Delta H_m = V_{mix}[(\Delta E_1^V/V_1)^{1/2} - (\Delta E_2^V/V_2)^{1/2}]^2 \Phi_1 \Phi_2 \quad (3)$$

where $V_{mix}$ is the volume of the mixture, $\Delta E_i^V$ is the energy of vaporization of species $i$, $V_i$ is the molar volume of species $i$, and $\Phi_i$ is the volume fraction of $i$ in the mixture. $\Delta E_i^V$ is the energy change upon isothermal vaporization of the saturated liquid to the ideal gas state at infinite volume [39].

The cohesive energy, $E$, of a material is the increase in the internal energy per mole of the material if all of the intermolecular forces are eliminated. The cohesive energy density (CED) Eq. (4), is the energy required to break all intermolecular physical links in a unit volume of the material [40]

$$CED = E/V = (\Delta H_{vap} - RT)/V \qquad (4)$$

where $\Delta H_{vap}$ is the enthalpy of vaporization.

The Hildebrand solubility parameter is defined as the square root of the cohesive energy density:

$$\delta = (E/V)^{1/2} \qquad (5)$$

Eq. (3) can be rewritten to give the heat of mixing per unit volume for a binary mixture:

$$\Delta H_m/V = (\delta_1 - \delta_2)^2 \Phi_1 \Phi_2 \qquad (6)$$

The heat of mixing must be smaller than the entropic term in Eq. (2) for polymer–solvent miscibility ($\Delta G_m \leq 0$). Therefore, the difference in solubility parameters ($\delta_1 - \delta_2$) must be small for miscibility or dissolution over the entire volume fraction range [39]. However, these predictions with the Hildebrand solubility parameters are made with the absence of any specific interactions, especially hydrogen bonds. They also do not account for the effects of morphology (crystallinity) and cross-linking. In addition, there may be (non-ideal) changes with changes in temperature and, in many cases, with changes in concentration.

One of the early schemes to overcome inconsistencies in the Hildebrand solubility parameter introduced by hydrogen bonding was proposed by Burrell [56], and is based on the assumption that solubility is greatest between materials with similar polarities. This method divided solvents into three categories depending on the hydrogen bonding: poor, moderate, and strong hydrogen bonding capabilities. The system of Burrell is summarized as follows: weak hydrogen bonding liquids are hydrocarbons, chlorinated hydrocarbons and nitrohydrocarbons; moderate hydrogen bonding liquids are ketones, esters, ethers, and glycol monoethers; and strong hydrogen bonding liquids are alcohols, amines, acids, amides, and aldehydes.

Hansen also accounted for molecular interactions and developed solubility parameters based on three specific interactions [38].

The first and most general type of interaction is the 'non-polar', also termed dispersive interactions, or forces. These forces arise because each atom consists of negatively charged electrons orbiting around a central positively charged nucleus. The moving negative charges create an electromagnetic field, which attracts all atoms to one another regardless of direction [57]. All molecules have this type of attractive force.

Polar cohesive forces, the second type of interaction, are produced by permanent dipole–dipole interactions. These polar forces roughly correlate with the dipole moment of the molecule

and the contribution to the dipole moment [40]. They are inherently molecular interactions and are found in most molecules to one extent or another.

The third major interaction is hydrogen bonding. Hydrogen bonding is a molecular interaction and resembles the polar interactions. These bonds are considerably weaker than covalent bonds but are much stronger than ordinary dipole–dipole interactions.

Therefore, as Hansen proposed, the cohesive energy has three components, corresponding to the three types of interactions:

$$E = E_D + E_P + E_H \qquad (7)$$

Dividing the cohesive energy by the molar volume gives the square of the Hildebrand solubility parameter as the sum of the squares of the Hansen dispersion (D), polar (P), and hydrogen bonding (H) components:

$$E/V = E_D/V + E_P/V + E_H/V \qquad (8)$$

$$\delta_2 = \delta_D^2 + \delta_P^2 + \delta_H^2 \qquad (9)$$

### 3.2. Estimation of solubility parameters

For low molecular weight substances (solvents), $\Delta H_{vap}$ can be calculated by a number of methods. Experimental values of $\Delta H_{vap}$ can be obtained using vapor pressure–temperature data or from heat capacity-temperature measurements. Numerical values for most solvents can be found in the literature. Therefore, estimating values of $\delta$ for low molecular weight solvents can be made.

When values of $\Delta H_{vap}$ are known at one temperature, they can be converted to the appropriate $\Delta H_{vap}$ values at any other temperature using the following empirical relationship first proposed by Watson [58,59]:

$$\Delta H_{vap,T_2}/\Delta H_{vap,T_1} = [(T_c - T_2)/(T_c - T_1)]^{0.38} \qquad (10)$$

This equation is useful because many liquids' $\Delta H_{vap}$ values, corresponding only to the normal boiling points, have been reported. Also, this expression is fairly accurate because the predicted $\Delta H_{vap}$ values are usually within about 2% of the experimental values [59].

Hildebrand developed another method to calculate $\Delta H_{vap}$ based on an empirical relationship which relates $\Delta H_{vap}$ at 25 °C to the normal boiling point, $T_b$, of non-polar liquids [50]:

$$\Delta H_{vap} = T_b^2 + 23.7T_b - 2950 \qquad (11)$$

The $\delta_D$ parameter can by calculated according to the procedures outlined by Blanks and Prausnitz [60]. They used the idea of homomorphs to obtain solubility parameters. For example, the homomorph of a polar molecule is a non-polar molecule having very nearly the same size and shape as that of the polar molecule in question. This concept is relatively easy to apply. The polar energy of vaporization is simply the difference between the experimentally determined total energy of vaporization and the energy of vaporization of the homomorph at the same reduced temperature [60]. Charts [61] can be used to find the energy of vaporization or cohesive energy, depending on whether the molecule of interest is aliphatic, cycloaliphatic, or aromatic.

The critical temperature, $T_c$, is required to make use of these charts. If the critical temperature cannot be found, it must be estimated. The $T_c$ values can be calculated from the Lyderson constants $(\sum \Delta_T)^1$, provided the boiling point $T_b$ at 1 atm is known, by

$$T_b/T_c = 0.567 + \sum \Delta_T - \left(\sum \Delta_T\right)^2 \qquad (12)$$

Blanks and Prausnitz calculated the polar solubility parameters by splitting the energy of vaporization of the polar fluid into non-polar and polar parts. However, these 'polar' parameters were actually the combined polar and hydrogen bonding parameters. These values were reassigned by Hansen and Skaarup [62] according to the Böttcher equation so that the real polar solubility component could be calculated by the equation

$$\delta_P^2 = [12\,108(\varepsilon - 1)(n_1^2 + 2)\mu^2]/[V^2(2\varepsilon + n_1^2)] \qquad (13)$$

where $\mu$ is the dipole moment (Debye), $\varepsilon$ is the dielectric constant, and $n_1$ is the refractive index of the liquid. Since most of these property constants are not reported for many compounds, Hansen and Beerbower [63] devised a simpler equation

$$\delta_P = 37.4\mu/V^{1/2} \qquad (14)$$

Until this point in time, the hydrogen bonding parameter was almost always found by subtraction of the polar and dispersion energies of vaporization from the total energy of vaporization. However, now the group contribution techniques are considered reasonably reliable for most of the required calculations and, in fact, more reliable than estimating several of the other parameters to ultimately arrive at the subtraction step just mentioned [38]. These techniques will be discussed later.

However, obtaining the solubility parameters for high molecular weight materials (polymers) is difficult because there is no measurable value of $\Delta H_{vap}$ or boiling point since polymers will degrade before they vaporize. Therefore, indirect methods must be used to obtain polymer solubility parameters, and these can be based on various kinds of measurements such as the determination of solubility relationships, of thermal changes accompanying mixing, and of various colligative properties such as vapor pressure, depression of the freezing point, and osmotic pressure. These measurements in conjunction with suitable theory can be used to evaluate $\delta$ for polymers [43]. Some widely used methods are

1. Directly measuring the solubility in a range of solvents or by measuring the degree of swelling of lightly crosslinked polymers. The extent of swelling will be a maximum when the $\delta$ value of the solvent matches that of the polymer.
2. Measuring the intrinsic viscosity of the uncrosslinked polymer in a series of solvents. The $\delta$ value for the solvent which produces the highest viscosity can be taken as the $\delta$ for the polymer. The best solvent gives the highest viscosity because the polymer chain is fully expanded and has the highest hydrodynamic volume.

However, these methods can be tedious and time consuming, so several alternative methods of calculation and calculating the values by group contributions have been explored extensively.

### 3.3. Group contribution methods of calculation of solubility parameters

Dunkel first considered $E$ as an additive property for low molecular weight materials [64]. He derived

group contributions for the cohesive energy of liquids at room temperature, and showed that $\Delta H_{vap}$ could be represented by the equation

$$\Delta H_{vap} = \sum \Delta h_i \tag{15}$$

where $\Delta h_i$ is the contribution of the $i$th atom or group to the molar heat of vaporization. Table 1 lists the values of $\Delta h_i$ reported by Dunkel for various atoms and groups. The solubility parameter may then be expressed as

$$\delta = \left[ \left( \sum \Delta h_i / V \right) - (RT/V) \right]^{1/2} \tag{16}$$

Small [65] proposed that the molar attractive constant, $F$, was a useful additive quantity for determining solubility parameters. He stated that the molar cohesive energy is given by

$$E = \Delta U_{vap} + \int_{V=V_{vap}}^{V=\infty} (\partial U/\partial V)_T \, dV \approx \Delta H_{vap} - RT \tag{17}$$

where $U$ is the internal energy. The integral is the correction for the imperfection of the vapor which is small when the vapor pressure is low (around 2% at 1 atm), and $E$ is about the same as the internal energy

Table 1
Values of $\Delta h_i$ reported by Dunkel for various atoms and groups

| Atom or group | $\Delta h_i$[a] (cal/mol) |
|---|---|
| CH$_3$ | 1780 |
| =CH$_2$ | 1780 |
| CH$_2$ | 990 |
| =CH | 990 |
| CH | $-380$ |
| O | 1630 |
| OH | 7250 |
| =CO | 4270 |
| CHO | 4700 |
| COOH | 8970 |
| COOCH$_3$ | 5600 |
| COOC$_2$H$_5$ | 6230 |
| NH$_2$ | 3530 |
| Cl | 3400 |
| F | 2060 |
| Br | 4300 |
| I | 5040 |
| NO$_2$ | 7200 |
| SH | 4250 |

[a] Values obtained from Ref. [43].

of vaporization. Since Scatchard [55] showed by the equation

$$E^{1/2}(n_1V_1 + n_2V_2)^{1/2} = n_1(E_1V_1)^{1/2} + n_2(E_2V_2)^{1/2}$$
(18)

that $(EV)^{1/2}$ is an additive property, Small considered it reasonable that it might add, in compounds, on an atomic and constitutive basis. It proved possible to find a set of additive constants for the common groups of organic molecules, which would allow the calculation of $(EV)^{1/2}$. Therefore, for one mole of the substance concerned, $\sum F$ summed over the groups present in the molecule of the substance gives the value of $(EV)^{1/2}$. Then

$$E = \left(\sum F\right)^2/V$$
(19)

$$\mathrm{CED} = \left(\sum F/V\right)^2$$
(20)

$$\delta = \sum F/V$$
(21)

Table 2 lists Small's molar attraction constants for several common functional groups or organic compounds, and Table 3 gives some values of the solubility parameters (for polymers) calculated from those constants in Table 2. These values were determined with the assumption that for the classes of compounds considered the dipole-interaction energy was negligible.

Rheineck and Lin [66] also developed another system of additive group increments and found that for homologous series of low molecular weight liquids, the contribution to the cohesive energy of the methylene group was not constant, but depended on the values of other structural groups in the molecule.

Hoy [67] combined vapor pressure data and group contributions to calculate the solubility parameters of a broad spectrum of solvents and chemical. His technique is as follows. First, the heat of vaporization at a given temperature from available vapor pressure data is given by the following Haggenmacher [68] equations

$$P(V_g - V_1) = (RT/M)[1 - (PT_c^3)/(P_cT^3)]^{1/2}$$
(22)

$$\Delta H = (\mathrm{d}P/\mathrm{d}t)(RT^2/MP)[1 - (PT_c^3)/(P_cT^3)]^{1/2}$$
(23)

Table 2
Small's molar attraction constants for several common functional groups or organic compounds

| Atom or group | $F^*$ (at 25 °C)[a] cal$^{1/2}$ c.c.$^{1/2}$ | Atom or group | $F^*$ (at 25 °C)[a] cal$^{1/2}$ c.c.$^{1/2}$ |
|---|---|---|---|
| CH$_3$ | 214 | CO ketones | 275 |
| CH$_2$ | 133 | COO esters | 310 |
| —CH— | 28 | CN | 410 |
| —C— | −93 | Cl (mean) | 260 |
| =CH$_2$ | 190 | Cl single | 270 |
| –CH= | 111 | Cl twinned as in >CCl$_2$ | 260 |
| >C= | 19 | Cl triple as in –CCl$_3$ | 250 |
| CH≡C– | 285 | Br single | 340 |
| –C≡C– | 222 | I single | 425 |
| Phenyl | 735 | CF$_2$ $n$-fluoro-carbons only | 150 |
| Phenylene ($o, m, p$) | 658 | CF$_3$ $n$-fluoro-carbons only | 274 |
| Naphthyl | 1146 | S sulphides | 225 |
| Ring, 5-membered | 105–115 | SH thiols | 315 |
| Ring, 6-membered | 95–105 | O·NO$_2$ nitrates | ∼440 |
| Conjugation | 20–30 | NO$_2$ (aliphatic nitro-compounds) | ∼440 |
| H (variable) | 80–100 | PO$_4$ (organic phosphates) | ∼500 |
| O ethers | 70 | | |

[a] Values obtained from Ref. [65].

Table 3
Values of the solubility parameters (for polymers) calculated from those constants in Table 2

| Polymer | $\delta_{(\mathrm{calc})}$[a] |
|---|---|
| Polytetrafluoroethylene | 6.2 |
| Polyisobutylene | 7.7 |
| Natural rubber | 8.15 |
| Polybutadiene | 8.38 |
| Polystyrene | 9.12 |
| Neoprene GN | 9.38 |
| Polyvinyl acetate | 9.4 |
| Polyvinyl chloride | 9.55 |
| Polyacrylonitrile | 12.75 |
| Polymethyl methacrylate | 9.25 |

[a] Values obtained from Ref. [65].

where $V_g$ is the specific volume of the gas phase, $V_l$ is the specific volume of the liquid phase, $M$ is the molecular weight, $P$ is the pressure, and $P_c$ is the critical pressure. Using these equations and the vapor pressure in the form of the Antoine equation

$$\log P = [-B/(T + C)] + A \tag{24}$$

where $P$ is in mm Hg, $T$ is in °C, and $A, B$, and $C$ are constants, the solubility parameter can then be calculated by the equation

$$\delta = \{(RT\rho/M)[1 - (PT_c^3)/(P_cT^3)]^{1/2}$$
$$\times [(2.303BT^2)/(T + C - 273.16)^2] - 1\}^{1/2} \tag{25}$$

where $\rho$ is density. However, the temperature of interest (usually 25 °C) can be beyond the range of the usual Antoine expression. This problem can be overcome by an alternate means of estimating the heat of vaporization at room temperature from data at different temperatures. At low pressures below atmospheric pressure the latent heat of vaporization follows the relationship:

$$\log \Delta H_{vap} = (-m/2.303)t + \log \Delta H_{vap}^0 \tag{26}$$

where $\Delta H_{vap}^0$ is the heat of vaporization at some standard temperature and $m$ is a constant. Using this relationship it is possible to estimate $\Delta H_{vap}$ at 25 °C by calculating the heat of vaporization in the temperature range in which the Antoine constants are valid and fitting these values into Eq. (26) to determine the slope $m$, and $\Delta H_{vap}^0$.

Hoy also re-examined Small's molar attraction constants using regression analysis, making corrections for acids, alcohol, and other compounds which are capable of association. Hoy assumed that carboxylic acids, for example, exist as dimers. Then the solubility parameter can be expressed as

$$\delta = (\Delta U\rho/M)^{1/2} \tag{27}$$

but for the case of dimeric carboxylic acids the actual molecular weight is twice that of the original and the solubility parameter becomes

$$\delta = (\Delta U\rho/M)^{1/2} \times (\sqrt{2})/2 \tag{28}$$

$E$ was calculated using the group contributions of Fedors [43] who found that a general system for estimating both $\Delta E_i^V$ and $V$ could be set up simply by

assuming

$$\Delta E_i^V = \sum \Delta e_i \tag{29}$$

and

$$V = \sum \Delta v_i \tag{30}$$

where $\Delta e_i$ and $\Delta v_i$ are the additive atomic and group contributions for the energy of vaporization and molar volume, respectively. In addition, it was found that both $\Delta E_i^V$ and $V$ for cyclic compounds could be estimated from the properties of linear compounds having the same chemical structure by adding a cyclization increment to both $\Delta E_i^V$ and $V$ of the linear compound.

However, a problem with the Fedors method arises when the substance has either a $T_g$ or $T_m$ above room temperature because the estimates of both $V$ and $\delta$ refer to the supercooled liquid rather than to the glass or to the crystalline phase. $V$ values are smaller and $\Delta E_i^V$ values are greater than experimental values. Therefore, small correction factors are introduced to alleviate this problem. For high molecular weight polymers with $T_g$s in this range, these correction factors are

$$\Delta v_i = 4n, \qquad n < 3 \tag{31}$$
$$\Delta v_i = 2n, \qquad n \leq 3 \tag{32}$$

where $n$ is the number of main chain skeletal atoms (including those in a ring system that is part of the chain's backbone) in the smallest repeating unit of the polymer. When polymers with $T_m$s above room temperature are concerned, the relationship between the molar volume of the liquid and crystalline phase, $V_c$, can be taken as

$$V = (1 + 0.13X)V_c \tag{33}$$

where $X$ is the degree of crystallization. Fedors noted that since the estimates of $\Delta E_i^V$ for a glass did not vary appreciably from that calculated for the liquid, one could assume that the $\Delta E_i^V$ for the glass and liquid were the same.

Using Eqs. (29) and (30)

$$\delta = \left( \sum \Delta e_i / \sum \Delta v_i \right)^{1/2} \tag{34}$$

and the limiting form for high molecular weight liquids becomes

$$\delta = \left(\sum \Delta e_{\mathrm{ir}} / \sum \Delta v_{\mathrm{ir}}\right)^{1/2} \tag{35}$$

Hoftzyer and Van Krevelen [69] compiled a set of group contribution values based on atomic contributions to calculate $F$ derived by Van Krevelen [70] and $E$ calculations based on Small's method. Their method estimates the individual solubility parameter components from group contributions using the following equations:

$$\delta_{\mathrm{D}} = \sum F_{\mathrm{Di}}/V \tag{36}$$

$$\delta_{\mathrm{P}} = \left(\sum F_{\mathrm{Pi}}^{2}\right)^{1/2}/V \tag{37}$$

$$\delta_{\mathrm{H}} = \left(\sum E_{\mathrm{Hi}}/V\right)^{1/2} \tag{38}$$

These parameters are then incorporated into Eq. (9) to calculate the Hildebrand parameter.

The prediction of $\delta_{\mathrm{D}}$ is the same type of formula used as Small first proposed for the prediction of the total solubility parameter, $\delta$. The group contributions $F_{\mathrm{Di}}$ to the dispersion component $F_{\mathrm{D}}$ of the molar attraction constant can simply be added. The same method holds for $\delta_{\mathrm{P}}$ as long as only one polar group is present. To correct for the interaction of polar groups within a molecule, the form of Eq. (37) has been chosen. The polar component is further reduced, if two identical polar groups are present in a symmetrical position. To take this effect into account, the value of $\delta_{\mathrm{P}}$, calculated with Eq. (37) must be multiplied by a symmetry factor of 0.5 for one plane of symmetry, 0.25 for two planes of symmetry, or 0 for more planes of symmetry. The $F$-method is not applicable to the calculation of $\delta_{\mathrm{H}}$. Hansen stated that the hydrogen bonding energy $E_{\mathrm{Hi}}$ per structural group is approximately constant, which leads to the form of Eq. (38). For molecules with several planes of symmetry, $\delta_{\mathrm{H}} = 0$ [68].

### 3.4. The $\chi$ parameter and its relation to Hansen solubility parameters

The Flory–Huggins parameter, $\chi$, has been used for many years in connection with polymer solution behavior, but it is desirable to relate this parameter to the Hansen solubility parameters (HSP). $\chi$ is an adjustable parameter that can be obtained from experimental measurements (e.g. from osmotic pressure measurement), but if the solubility parameters of the system are known, they can be used to estimate $\chi$ as follows

$$\chi_{\mathrm{sp}} = 0.34 + V_{\mathrm{s}}/RT(\delta_{\mathrm{s}} - \delta_{\mathrm{p}}) \tag{39}$$

The 0.34 is a factor which is necessary to preserve the Flory form of the chemical potential expression. The most likely origin of this correction term lies in so-called free volume effects that are neglected in the Flory–Huggins treatment. In the liquid state, the motion and vibrations of the molecules lead to density fluctuations, or free volume. The free volume associated with a low molecular weight liquid is usually larger than that of a polymer so that in mixtures of the two there is a mismatch of free volumes. This leads to the need for an additional term. In fact, a more general way of expressing the Flory $\chi$ term is to let it have the form:

$$\chi = a + b/T \tag{40}$$

where the quantity $a$ can be thought of as an entropic component of $\chi$, accounting for non-combinatorial entropy changes such as those associated with free volume, while $b$ is the enthalpic part [71].

### 3.5. Techniques to estimate Hansen solubility parameters for polymers

For low molecular weight, non-polymeric substances, $\Delta H_{\mathrm{vap}}$ can be calculated by a number of methods or easily found in the literature and handbooks, so estimation of $\delta$ is simple. However, this is not the case for macromolecules. Polymers do not vaporize so there is no real value of $\Delta H_{\mathrm{vap}}$ and $\delta$ becomes difficult to determine. Therefore, experimental methods to determine the HSP have been developed.

The simplest method is to evaluate whether or not the polymer dissolves in selective solvents, or evaluate their solubility or degree of swelling/uptake in a series of well-defined solvents [38]. The solvents should have different HSP chosen for systematic exploration of the three parameters at all levels. The middle of the solubility range (in terms of $\delta_{\mathrm{s}}$) or the maximum of swelling is taken as the $\delta_{\mathrm{p}}$.

Another solubility characterization method is that of using the intrinsic viscosity. The intrinsic viscosities will be higher in better solvents because of greater interactions and greater polymer chain extensions (viscosity $\propto$ hydrodynamic volume of the chain in solution). The $\delta_s$ of the solvent which gives the maximum dilute solution viscosity is taken as the $\delta_p$ of the polymer.

There are other more complicated techniques to evaluate polymer solubility parameters such as permeation measurements, chemical resistance determinations of various kinds, and surface attack. These usefulness and accuracy of experimental techniques depends on the polymer involved. Others can be problematic because of the probable influence of factors such as solvent molar volume and length of time before attainment of equilibrium [38].

### 3.6. Predicting polymer solubility

Solubility behavior cannot be accurately predicted by only the Hildebrand solubility parameter. As mentioned earlier, solubility can be affected by any specific interactions, especially H-bonds, polymer morphology (crystallinity) and cross-linking, temperature, and changes in temperature. Also of importance is the size and shape of the solvent molecules. Therefore, several graphing and modeling

techniques have been developed to aid in the prediction of polymer solubility [72].

Crowley et al. [73] developed the first three-component graphing system using the Hildebrand parameter, a hydrogen bonding number, and the dipole moment. A scale representing each of these three values is assigned to a separate edge of a large empty cube. Then, any point within the cube represents the intersection of three specific values: the Hildebrand value, dipole moment, and hydrogen bonding value (Fig. 3) [72]. Once all the solvent positions are determined, solubility tests are performed on polymers. The positions of solvents that dissolve a polymer are indicated by black balls, non-solvents by white balls, and partial solubilities by gray balls. Therefore, a three-dimensional volume of solubility is outlined with liquids within the volume being active solvents and liquids outside the volume being non-solvents. The gray balls create the interface. The 3D plot can then be translated into a 2D plot (Fig. 4) [72,74] by plotting the data on a rectangular graph that represents only two of the three component parameter scales. The polymer solubility volume becomes an area which represents either a single slice through the volume at a specified value on the third component parameter scale or a topographic map that indicates several values of the third parameter at the same time.
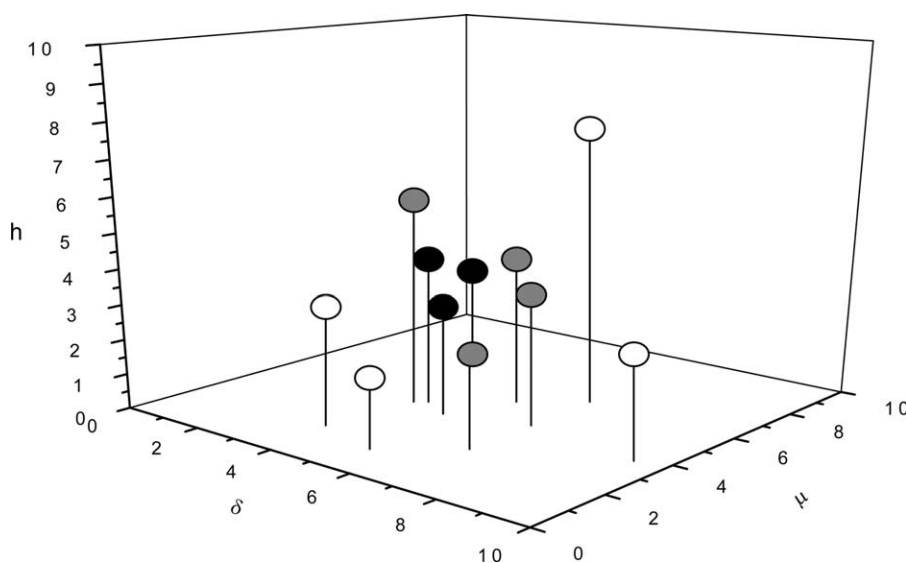


Fig. 3. A three-dimensional box used to plot solubility information by Crowley, Teague, and Lowe with axes representing the Hildebrand solubility parameter, $\delta$, the dipole moment, $\mu$, and hydrogen bonding value, $h$. (Adapted from Refs. [71,72].)
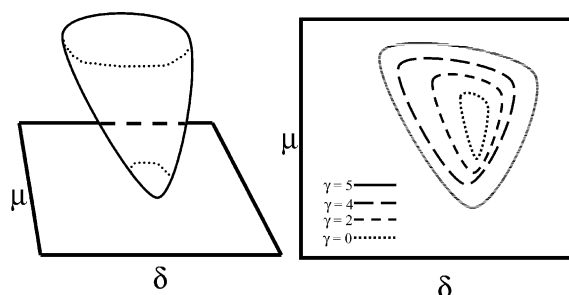
Fig. 4. Approximate 2D representations of solid model and solubility map for cellulose acetate. (Adapted from Refs. [71,73].)

A second modeling technique of 3D solubility was developed by Hansen [38,75]. The Hansen characterization is usually considered as a sphere. The center of the sphere has the $\delta_D$, $\delta_P$, and $\delta_H$ values of the polymer in question (solute). The radius of the sphere, $R_o$, is termed the interaction radius. The boundary of the spherical characterization is based on the requirement that 'good' solvents have a distance from the center of the sphere, $R_a$ (also termed the solubility parameter distance) less than $R_o$. $R_a$ is given by the relation

$$R_a^2 = 4(\delta_{D,p} - \delta_{D,s})^2 + (\delta_{P,p} - \delta_{P,s})^2 + (\delta_{H,p} - \delta_{H,s})^2 \tag{41}$$

where $\delta_{D,p}$, $\delta_{P,p}$, and $\delta_{H,p}$ are the Hansen solubility components for the polymer, and $\delta_{D,s}$, $\delta_{P,s}$, and $\delta_{H,s}$ are the Hansen solubility components for the solvent. Eq. (41) was developed from plots of experimental data where the constant '4' was found convenient and correctly represented the solubility data as a sphere encompassing the good solvent. This constant is theoretically predicted corresponding states theory of polymer solutions by the Prigogine when the geometric mean is used to estimate the interaction in mixtures of dissimilar molecules [38,76]. A convenient single parameter to describe solvent quality is the relative energy difference, RED, number:

$$RED = R_a/R_o \tag{42}$$

An RED number of 0 is found for no energy difference. RED numbers less than 1.0 indicate high affinity; RED equal to or close to 1.0 is a boundary condition; and progressively higher RED numbers indicate progressively lower affinities [38]. Fig. 5 is a sketch of a sphere of solubility in the Hansen three-dimensional solubility parameter system [75].

The Hansen characterization can also be represented in two dimensions by plotting a cross-section through the center of the solubility sphere on a graph that used only two of the three parameters, if need be.
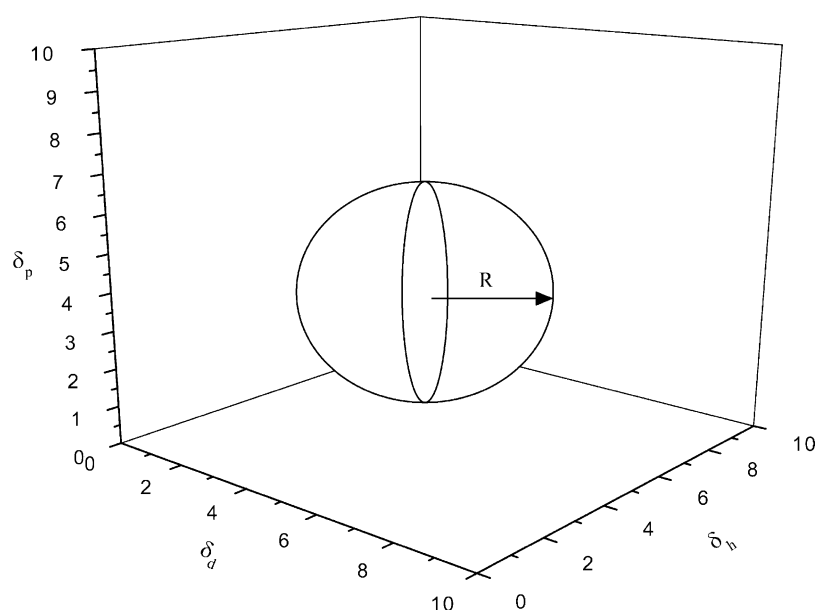


Fig. 5. Sketch of a sphere of solubility in the Hansen three-dimensional solubility parameter system. (Adapted from Ref. [74].)

Also, this method has also been used to predict environmental stress cracking [77].

It is important to note that deviations can occur with this method. These are most frequently found to involve the larger molecular species being less effective solvents compared with the smaller counterparts which define the solubility sphere. Likewise, smaller molecular species such as acetone, methanol, nitromethane, and others often appear as outliers in that they dissolve a polymer even though they have solubility parameters placing them at a distance greater than the experimentally determined radius of the solubility sphere. Smaller molar volume favors lower free energy of mixing, which promotes solubility. Such smaller molecular volume species which dissolve 'better' than predicted by comparisons based on solubility parameters alone should not necessarily be considered non-solvents [38].

The sizes of both the solvent and polymer can affect solubility due to differences in diffusion, permeation, and chemical resistance. Smaller molecules will tend to dissolve more easily than larger ones. Molecular shape can also be important. Smaller and more linear molecules diffuse more rapidly than larger more bulky ones. All these factors must be kept in mind when predicting solubility.

Another method developed to predict polymer solubility was developed by Teas [78]. Using a set of fractional parameters mathematically derived from the three Hansen parameters, a 2D graph is obtained. This method is based on a hypothetical assumption that all materials have the same Hildebrand value. According to this assumption, solubility behavior is determined, not by differences in total Hildebrand value, but by the relative amounts of the three component forces that contribute to the total Hildebrand value [72]. The fractional parameters used by Teas are mathematically derived from Hansen values and indicate the percent contribution that each Hansen parameter contributes to the Hildebrand value

$$f_D = \delta_D/(\delta_D + \delta_P + \delta_H) \tag{43}$$

$$f_P = \delta_P/(\delta_D + \delta_P + \delta_H) \tag{44}$$

$$f_H = \delta_H/(\delta_D + \delta_P + \delta_H) \tag{45}$$

and

$$f_D + f_P + f_H = 1 \tag{46}$$
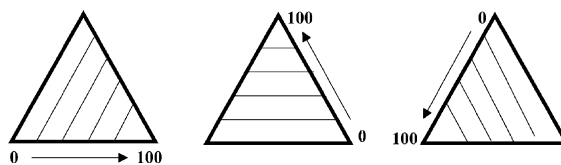


Fig. 6. The Teas graph is an overlay of three solubility scales. (Adapted from Ref. [74].)

These values can then be plotted on triangular graphs on which three axes oriented at 60° (Fig. 6) [72]. This construction derives from the overlay of three identical scales each proceeding in a different direction. Therefore, alkanes, for example, whose only intermolecular bonding is due to dispersion forces are located in the far lower right corner of the Teas graph. This corner corresponds to a contribution by the 100% dispersion forces and 0% contribution from polar or hydrogen bonding forces. Moving toward the lower left corner, corresponding to 100% hydrogen bonding contribution, the solvents exhibit increasing hydrogen bonding capability culminating in the alcohols and water molecules with relatively little dispersion force compared to their very great hydrogen bonding contribution [72]. An example of a Teas graph with several solvent groups can be seen in Fig. 7 [72].

Once the positions of the solvents are determined on the triangular graphs, it is possible to obtain polymer solubilities using methods similar to those of Crowley and Hansen. A polymer is tested in the various solvents whose positions have been determined, and the degree of swelling and/or dissolution is monitored. For example, liquids determined to be good solvents might have their positions marked with a blue mark, marginal solvents might be marked with a green mark, and non-solvents marked with red.
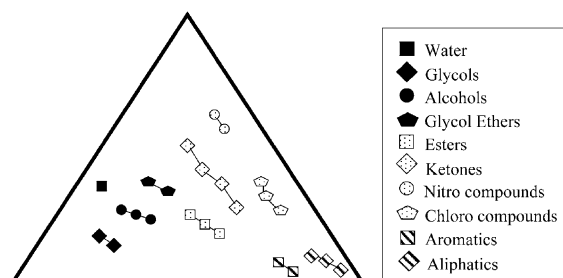


Fig. 7. A Teas graph with solvents grouped according to classes. (Adapted from Ref. [74].)

Once this is done, a solid area on the Teas graph will contain all the blue marks, surrounded by green marks. The edge of this area is termed the polymer solubility window.

This method is particularly useful in selecting solvent mixtures for specific applications. Solvents can be mixed to selectively dissolve one material but not another; control evaporation rate, solution viscosity, degree of toxicity or environmental effects; and, in some cases, decrease cost.

The solubility parameter of a liquid mixture can be calculated by incorporating the volumewise contributions of the solubility parameters of the individual components of the mixture. The fractional parameters for each liquid are multiplied by the fraction that the liquid occupies in the blend, and the results for each parameter are added together. In this way, the position of the solvent mixture can be located on the Teas graph according to its fractional parameters. Calculations for mixtures for three or more solvent are made in the same way. This method is also useful for predicting solubility with mixtures of non-solvents. For example, two non-solvents for a specific polymer can sometimes be blended is such a way that the mixture will act as a good solvent. This is possible if the graph position of the mixture lies inside the solubility window of the polymer and is most effective if the distance of the non-solvent from the edge of the solubility window is small [72].

These are a selection of the graphing/mapping/-modeling techniques that have been developed to aid in the understanding and prediction of polymer solubility. Extensive descriptions of other polymer maps and models can be found in Ref. [79].

## 4. Polymer dissolution models

The dissolution mechanism of an amorphous polymer is highlighted in Fig. 8. The glassy polymer starts with a layer thickness of $2l$. At the beginning of the dissolution process, the solvent penetrates and swells the polymer causing a transition from the glassy to a rubbery state, and two interfaces are formed: a swelling interface at position R and a gel–solvent interface at position S. As R moves inwards toward the center of the slab, S moves in the opposite direction. After an induction time which terminates
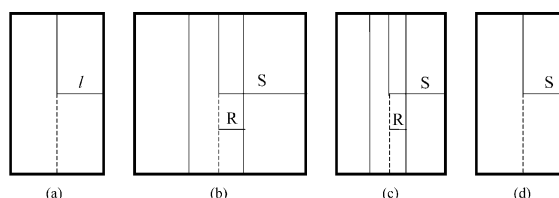


Fig. 8. Schematic representation of a one-dimensional solvent diffusion and polymer dissolution process. (a) Initial slab of thickness $2l$; (b) initial swelling step showing the increasing position of the rubbery–solvent interface (S) and the decreasing position of the glassy–rubbery interface (R); (c) onset of the dissolution step showing the decreasing position of the interface S along with the decreasing position of the interface R; (d) final dissolution step where the slab has been transformed into a rubbery material (disappearance of interface R) and the position of interface S still decreases. (Adapted from Ref. [104].)

when the concentration of the penetrant in the polymer exceeds a critical value, chain disentanglement begins, and true dissolution occurs. After the glassy core disappears as R continues inward, only front S exists, and it continues to move inwards until polymer dissolution is complete. This is the general understanding of the mechanism of polymer dissolution.

Several other models have been formulated to explain the experimentally observed dissolution behavior and have been reviewed [2,80–82]. There are five main approaches to modeling amorphous polymer dissolution [2,81]:

1. *Phenomenological models with Fickian equations.* These models attempt to physically describe the dissolution process using Fickian conditions and the moving boundaries present in the system.
2. *Models with external mass transfer as the controlling resistance to dissolution.* These models assume that the controlling factor in dissolution is resistance due to an external mass transfer.
3. *Stress relaxation models and molecular theories.* These models predict the polymer relaxation response to solvent uptake.
4. *Analysis using transport models for swelling and scaling laws for chain disentanglement.* These models are used to calculate polymer dissolution in the anomalous transport and scaling models.
5. *Continuum framework models.* These take into account the viscoelastic effects and mobility changes of the polymer during dissolution while

using anomalous transport models to predict the behavior of solvent diffusion.

This section concentrates on several proposed models of glassy polymer dissolution and is divided into subsections based on the five classifications of these models. A few selected examples of controlled release models as also discussed, but a complete, more detailed discussion of these systems is discussed elsewhere [80].

## 4.1. Phenomenological models

### 4.1.1. The multi-phase Stefan problem

Tu and Ouano [83] proposed one of the first models for polymer dissolution, assuming Fickian solvent diffusion into the polymer followed by the establishment of two distinct boundaries characterized by sharp changes in the concentration of the solvent. They also assumed that the conditions of constant chain disassociation concentration and rate are established immediately upon wetting the polymer surface and that the solvent and the polymer are incompressible. The first boundary between the liquid solvent and gel-like solution phase provides a partition between the dissolved and undissolved polymer, and the concentration at this interface is a defined quantity for a given polymer–solvent pair. At the liquid–gel interface, the polymer molecules go from the gel-like phase (entangled state) to a less viscous liquid solution (free state) at a rate defined as the disassociation rate, $R_d$, which may be experimentally estimated by extrapolating the solubility rate to very high solvent velocity across the liquid–gel interface. The second boundary (also characterized by concentration) lies between the gel-like and the glass-like phases and is also marked by a change in the diffusion coefficient of the solvent in the polymer matrix. Once the concentrations at these interfaces are defined and the different material parameters such as the diffusion coefficients of the solvent and polymer and $R_d$ are known, the kinematics of dissolution can be formulated and the spatial locations of the liquid–gel and polymer–glass interfaces tracked with time. Therefore, assuming the model is correct and the parameters used are accurate, the kinematics of the swelling and the dissolution of the polymer can be described analytically.

It was proposed that the dissolution process is disassociation-controlled if the polymer diffusion rate in a liquid layer adjacent to the polymer–gel interface is faster than the disassociation rate, or diffusion-controlled if the diffusion rate is slower than the disassociation rate. The solvent diffusional flux, $j_s$, is defined by the diffusion coefficient of the solvent, $D_s$, a function of $\phi_p$, $f_s(\phi_p)$, and the position of the solvent–gel interface, $S(t)$, as follows:

$$x < S(t), \qquad j_s = -D_s f_s(\phi_p)(\partial \phi_s / \partial x) \tag{47}$$

As the solvent penetrates the polymer, the polymer swells at a rate,

$$v_s = -j_s(x, t) \tag{48}$$

and the interface position is derived as

$$dS/dt = v_s - R_d \tag{49}$$

The swelling velocity is equal in magnitude but opposite in direction to the solvent flux, forming the two interfaces. The flux of polymer, $j_p$, at the gel–liquid interface is dependent on the movement of that interface and defined as

$$x > S(t), \qquad j_p = -D_p f_p(\phi_p)(\partial \phi_p / \partial x) \tag{50}$$

The disassociation rate, $R_d$, is assumed to be equal to the diffusion of the dissolved polymer into the bulk liquid, i.e.

$$R_d = j_p(x, t) \tag{51}$$

As a result, the governing solvent diffusion equation in the polymer in the region between the solvent–gel interface, $S$, and the external polymer thickness, $L$, is

$$S < x < L,$$
$$\partial \phi_p / \partial t = D_s \, \partial/\partial x [f_s(\phi_p) \phi_p \, \partial \phi_p / \partial x] \tag{52}$$

The governing polymer diffusion equation in the liquid boundary layer is derived as

$$x < S(t),$$
$$\partial \phi_p / \partial t + dS/dt \, \partial \phi_p / \partial x = D_p \, \partial/\partial x [f_s(\phi_p) \partial \phi_p / \partial x] \tag{53}$$

The equation for the interface position, S, is

$$dS/dt = D_p f_p(\phi_p) \partial \phi_p / \partial x - D_s f_s(\phi_p) \partial \phi_s / \partial x \tag{54}$$

It is assumed that at small times, the solvent flux into the polymer is sufficient to carry away all the chains that dissolved from the gel into the liquid, and the dissolution is disassociation-controlled. When the solvent concentration at the gel–liquid boundary reaches a constant concentration, the flux is no longer sufficient to carry all of the dissolved chains away from the surface, at which time the dissolution becomes diffusion-controlled.

From existing data for the dissolution of PS in MEK, this mathematical model was verified experimentally by an in situ technique measuring the motions of the polymer–gel and the liquid–gel interfaces. Different forms of the functions $f_s$ and $f_p$ were used in the simulations, and it was shown that the concentration dependence of the diffusion coefficient is crucial. The disassociation rate, $R_d$, was treated as a model parameter, and the simulations failed to yield more insight into the actual rate. Another weakness of the model is that no mechanism for the disassociation of the polymer from gel is provided. In addition, the contribution of reptation time to the delay in the onset of dissolution is neglected, and the assumption of constant solvent concentration at the gel–liquid interface disregards the possible effects of solvent history on the dissolution process.

### 4.1.2. Disengagement dynamics

Devotta et al. [84] predicted the lifetime of a dissolving polymeric particles in a hydrodynamic field by building a model that included the phenomenon of reptation of the polymer chains, disengagement of these chains from the gel–liquid interface, and, also, diffusion in the boundary layer surrounding the gel–liquid interface. In this model the minimum time for a polymer to reptate out of the entangled swollen network and disengage itself from the interface is assumed to be equal to the reptation time, $t_{rep}$, which is primarily dependent on the structure of the polymer and molecular weight. Polymer chains, being long and mutually entangled, are inhibited from entering the liquid phase due to the dynamic friction between the chains. It was proposed that the rate at which the polymer chains disengage themselves from the gel–liquid interface is one of the factors controlling the dissolution rate in polymeric systems. In addition to the disengagement process at

the interface, there is some mass transfer resistance at the surface due to a concentration gradient that is established between the interface of the swollen gel and the bulk liquid, which drives this process. When the disengagement rate, $R_d$, is relatively low, the resistance of the eternal boundary layer, quantified by the mass transfer coefficient, $k_l$, is neglected. However, if the surface disengagement and the subsequent transport of the disengaged chains occurs at comparable rates, then, depending on the relative magnitude of the resistances at any instance, the dissolution process is disengagement limited or diffusion limited. The assumption is made that the glass–gel transition is rapid and the details of the kinetics of the glass–gel transition process are neglected. The solvent transport is described through a Fickian equation as

$$t > 0, \quad 0 < r < S(t),$$

$$\partial \phi_s / \partial t = (1/r^2) \partial / \partial r (r^2 D_s \, \partial \phi_s / \partial r) - (1/r^2) \partial / \partial r (r^2 \nu_s \phi_s)$$

$$(55)$$

where $r$ the radial position. The initial and boundary conditions for the above equations are

$$t = 0, \quad 0 < r < r_0 \, \phi_s = 0 \tag{56}$$

$$r = R(t), \quad t > 0 \, \phi_s = \phi_{s,eq} \tag{57}$$

$$r = 0, \quad t > 0 \, \partial \phi_s / \partial r = 0 \tag{58}$$

where $r_0$ is the initial radius of the polymeric particle and $\phi_{s,eq}$ the equilibrium volume fraction of the solvent in the polymer, which is assumed to be constant as per convention and greater than the critical concentration required for disengagement.

The position of the moving boundary is given by

$$dS/dt = (D_s \, \partial \phi_s / \partial r)_{r=S^-(t)} - (D_p / \phi_{p,eq})(\partial \phi_p / \partial r)_{r=S^+(t)}$$

$$(59)$$

where $\phi_{p,eq}$ is the equilibrium volume fraction of polymer in the solvent. The first term on the right-hand side is due to the swelling of the polymer network, and the second is due to the dissolution.

To model the chain disengagement, the following boundary condition is written on the liquid side of the liquid–gel interface

$$r = S^+(t), \quad 0 < t < t_{rep},$$

$$-D_p(\partial \phi_p / \partial r) = 0 \tag{60}$$

$$r = S^+(t), \qquad t > t_{\text{rep}},$$
$$\hspace{8cm} (61)$$
$$-D_{\text{p}}(\partial \phi_{\text{p}}/\partial r) = k_{\text{d}} \phi_{\text{p,eq}}$$

where $k_{\text{d}}$ is defined as the disengagement rate. For transport in the liquid, mass transfer is assumed to be the dominating resistance, and, hence, at the liquid side of the liquid–gel interface, as long as $\phi_{\text{p}} = \phi_{\text{p,eq}}$,

$$r = S^+(t), \qquad t > t_{\text{rep}},$$
$$\hspace{8cm} (62)$$
$$-D_{\text{p}} \, \partial \phi_{\text{p}}/\partial r = k_{\text{s}}(\phi_{\text{p,eq}} - \phi_{\text{p,b}})$$

where $k_{\text{l}}$ is the liquid side mass transfer coefficient, and $\phi_{\text{p,b}}$ is the polymer volume fraction in the bulk. Correlations are used to obtain the mass transfer coefficient. The model equations are made dimensionless by suitable transforms and solved using a Crank–Nicholson scheme. Therefore, the resistance offered due to mass transfer controls the diffusion of the chains away from the gel–liquid interface. At times just greater than the reptation time of the polymer, dissolution is predicted to be disengagement-controlled. On the other hand, at longer times the mechanism is predicted to change to diffusion-controlled.

Studies with a PS–cyclohexane system were conducted to verify the validity of the model. The experiments demonstrated that there is a critical size of a polymer particle below which the time of dissolution of a solid polymer particle remains almost independent of the particle size. This critical size increased with an increase in the rate of stirring as shown in Fig. 9. The comparison between the semi-quantitative predictions and experimental observations were reasonably good (Fig. 10).

Ranade and Mashelkar [85] took this model one step further by considering the dissolution of a spherical polymeric particle in a convective field. The swelling rate, $v_{\text{s}}$, is related to the diffusion of the solvent and the polymer in the gel phase as

$$v_{\text{s}} = 1/Pe_{\text{R}}(D_{\text{pg}} \, \partial \phi_{\text{p}}/\partial r + D_{\text{sg}} \, \partial \phi_{\text{s}}/\partial r) \hspace{1cm} (63)$$

where $D_{\text{pg}}$ and $D_{\text{sg}}$ are dimensionless diffusivities of the polymer and the solvent in the gel phase, respectively. $Pe_{\text{R}}$ is the Peclet number. The boundary conditions are similar to those defined by Devotta et al.
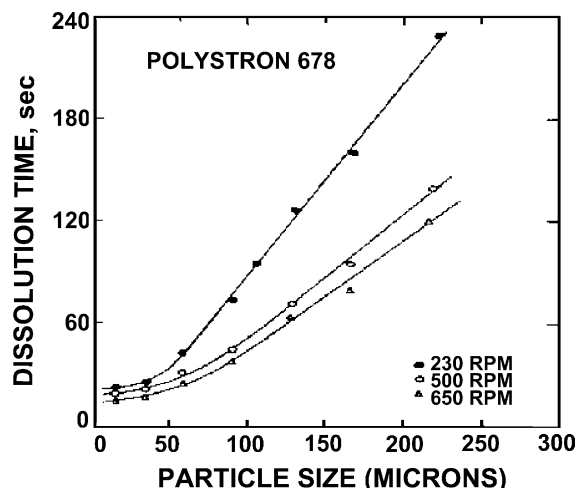


Fig. 9. Dissolution time as a function of the average particle size of polystyrene particles in cyclohexane at different stirring speeds ($T = 35°$). (Adapted from Ref. [84].)

[84], and the effective disengagement rate, $k_{\text{eff}}$, is treated as a model parameter.

If the dissolving polymer particles are placed in a uniform stream of solvent moving with velocity $v_{\text{s}\infty}$, then the polymer concentration field will not be uniform in the $r$ and $\theta$ directions. Therefore, the transport equations must be solved in both the $r$ and $\theta$ directions. The $r$ component of the mass balance in Eq. (55) is written as
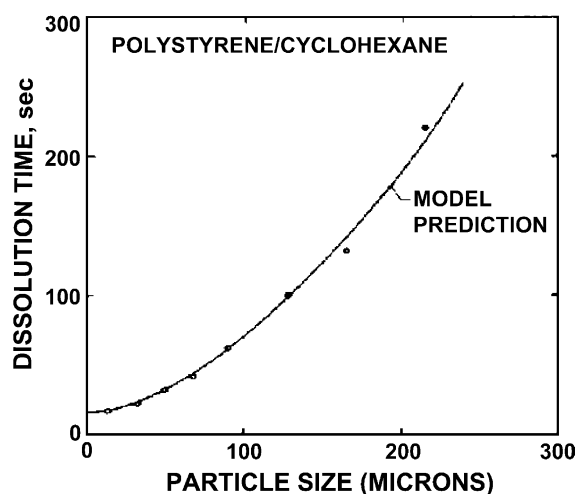


Fig. 10. Comparison of the model prediction with the experimental data for PS–cyclohexane. (Adapted from Ref. [84].)

$$\alpha(\partial\phi_p/\partial t)+1/r^2\partial/\partial r(r^2 v_r\phi_p)+(1/r\sin\theta)\partial/\partial\theta$$

$$\times(v_\theta\sin\theta\phi_p)=1/Pe_R\{1/r^2\partial/\partial r(r^2 D_p\partial\phi_p/\partial r)$$

$$+(1/r^2\sin\theta)\partial/\partial\theta(D_p\sin\theta\partial\phi_p/\partial\theta)+S_\phi$$

$$(64)$$

where $\alpha$ is the ratio of the reference length scale to the product of the reference time and the reference velocity scales, $v_r$ is the $r$-component of the velocity and $v_\theta$ is the $\theta$-component of the velocity, and $S_\phi$ is the source term.

The creeping flow solution, with slight modification in radial velocity (assuming $\theta$ independent swelling velocity, $v_{sp}$) due to swelling, can be used to estimate the external velocity field as

$$v_r=[1-1.5(r/S)+0.5(r/S)^3]\cos\theta+v_{sp}/(r/S)^2 \quad (65)$$

$$v_\theta=-[1-0.75(r/S)-0.25(r/S)]\sin\theta \quad (66)$$

where $v_{sp}$ is the velocity of the gel–solvent interface.

Analysis of the computed results for a wide range of parameters suggested that the value of reptation time, $t_{rep}$, and of the solvent diffusivity in the gel phase $D_s$, govern the formation and swelling process of the gel phase. Fig. 11 shows the typical movement of the glass–gel and gel–liquid interface during the dissolution process. The radius of the glassy region decreases continuously, and at times less than $t_{rep}$, the solid polymer particle only swells, and at times equal to $t_{rep}$,

the macromolecules start disengagement at the gel–liquid interface. It can be seen that although glass transition kinetics influences the duration of the glassy phase in the polymer particle, the dissolution time remains almost unaffected. Radial profiles of the polymer volume fraction during the dissolution process are shown in Fig. 12 and indicate that the particle becomes saturated in the late stages of dissolution.

The effects of the diffusivity of the polymer in the solvent, $D_p$, the external velocity, $v_{s\infty}$, and the disengagement rate, $k_d$, on dissolution time is shown in Fig. 13, and the resulting trends are as follows. First, for larger particle sizes, the dissolution times decrease as the particle size decreases, and as the diffusivity of the polymer increases. The dissolution time decreases because of the enhanced mass transfer rate. Second, an increase in the external velocity, $v_{s\infty}$, causes a decrease in dissolution time, and the dissolution time varies linearly with particle size. Lastly, when the disengagement rate is very slow (compared to external mass transfer), the dissolution process is not influenced by mass transfer, and the dissolution time varies nearly linearly with the particle size.

Several limiting cases were also examined: glass transition-controlling, disengagement process-controlling, external mass transfer process-controlling,



Fig. 11. Movement of glass–gel and gel–solvent interfaces during the dissolution process. $D_p/D_s=0.2$, $R_0=2$, $k_d=5$, $Pe=5000$, $f_{p,b}=0.5$. (Adapted from Ref. [85].)
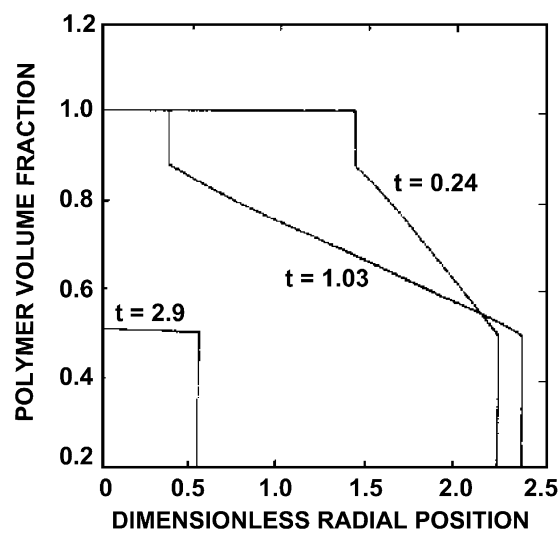


Fig. 12. Radial profiles of the polymer volume fraction during dissolution. Theoretical predictions have been adapted from the work of Ranade and Mashelkar, using the following parameters: $k_d/v_R=1000$, $D_p/D_1=0.2$, $R_0=2$, $k_d=5$, $Pe=5000$, $f_{p,b}=0.5$. (Adapted from Ref. [85].)
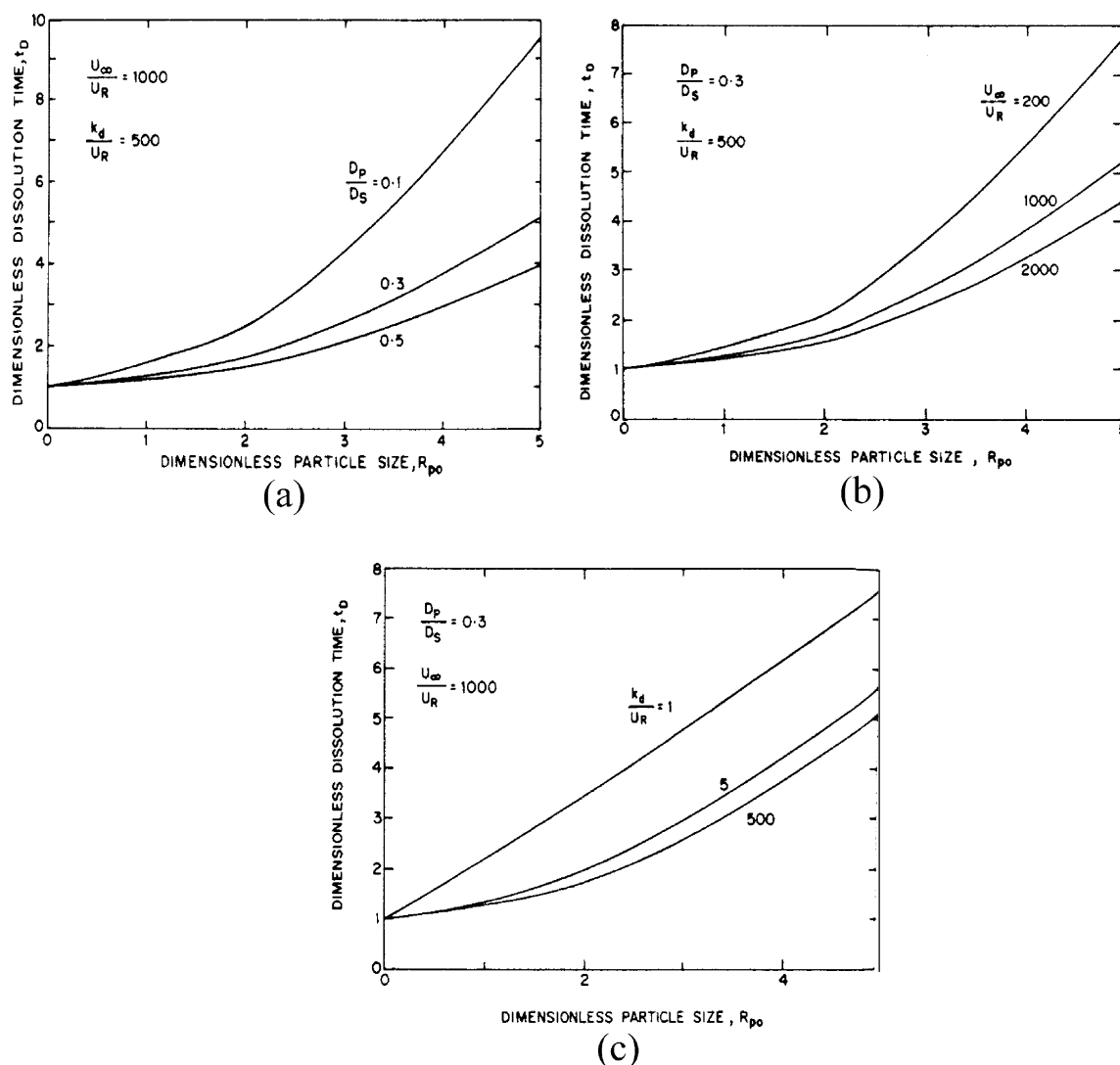
Fig. 13. Effect of (a) parameter $D_p/D_s$; (b) disengagement rate; (c) external velocity on the dissolution time for different particle sizes. Reprinted with permission from AIChE J 1995;41(3):666–76. © 1995 American Institute of Chemical Engineers [85].

and reptation process-controlling. The first controlling factor, glass transition, was inspected by analyzing the dissolution model without the overlying assumption that the glass–gel transition occurred quickly. Then the glass transition occurred slowly when compared to the eternal mass transfer and disengagement rates, no gel layer was predicted, and the dissolution time of the spherical particle was predicted to be proportional to its radius.

In the second case where the controlling factor was the disengagement rate, the glass transition was assumed to occur rapidly and the gel layer always existed. This was presumed to be the case modeled when the external flow was rapid, leading to a high rate of mass transfer from the interface. Here, the dissolution time for the particle was again determined to be proportional to the radius of the dissolving polymer particle.

When the glass transition and disengagement rates are fast enough to make the external mass transfer controlling, the system is treated as a non-polymeric solid, and the dissolution rate varies as a function of the radius of the particle to the five-third of the power.

The dissolution process is controlled by reptation if the particle is very small and the disengagement rate and diffusion through the boundary layer are high. In this case, the dissolution time will be equivalent to the reptation time.

The predictions of both models were compared with experiments performed with PMMA–benzene system (Fig. 14), and good agreements were observed. The figure shows that there is indeed a critical particle size below which the dissolution time of the polymer is constant. This observation is, in contrast with the dissolution behavior of small molecular weight solutes, where the dissolution time vanishes as the particle tends to zero.

The model was further modified by Devotta et al. [86] with the belief that the presence of a small amount of residual solvent enhances the mobility of the polymer chains substantially apart from enhancing the diffusion of the solvent into it. The diffusion equation in the polymer matrix in terms of the polymer volume fraction, $\phi_p$, takes the following form

$$R < x < S, \qquad \partial \phi_p / \partial t = \partial/\partial x (D_s \phi_p \, \partial \phi_p / \partial t) \qquad (67)$$

The free volume model of Zielinski and Duda [87] is used to model the concentration dependence of



Fig. 14. Experimental data for PMMA ($M_w = 82\,000$)-benzene system vs. model predictions. (Adapted from Ref. [85].)

the diffusion coefficient. The kinetics of glass transition of the glassy polymer to a gel-like state is expressed as

$$dR/dt = K(\phi_{s|x=R} - \phi_{s,t})^n \qquad (68)$$

Here, $\phi_{s|x=R}$ is the concentration of the solvent at the interface of the swollen and glassy polymer and $\phi_{s,t}$ is the concentration level corresponding to the threshold activity for swelling. Also, $K$ and $n$ are the swelling kinetic parameters of the model.

As the polymer chains disengage, the boundary erodes and the polymer molecules move out from the gel-like phase through a diffusion boundary layer. The transport of the polymer chains across the boundary layer is described by the following conservation equation

$$\partial \phi_p / \partial t = \partial/\partial x (D_p \, \partial \phi_p / \partial x) - dR/dt \, \partial \phi_p / \partial x \qquad (69)$$

The appropriate initial and boundary conditions are written by assuming that no polymer disengages from a time equal to the reptation time of the chain and after a time equal to the reptation time elapses, and the chains disengage at a finite rate, $k_d$.

The gel–liquid interface moves as the result of solvent transport and polymer disengagement, and is described by

$$dS/dt = (D_s \, \partial \phi_p / \partial x)_{x=S^-(t)} - ((D_p/\phi_{p,eq}^-) \partial \phi_p / \partial x)_{x=S^+(t)} \qquad (70)$$

In Eq. (70), the first term on the right-hand side represents the increase in dimension of the polymer particle due to swelling, and the second term represents the decrease in length due to the disengagement at the interface. It was proposed that the disengagement rate is proportional to the mobility of the disengaging polymer chain, $m_p$. The rate of change of mobility is assumed to be given by a product of kinetic constant and the extent of departure from the maximum mobility. This mobility depends on the concentration of solvent and hence on the fractional free volume of the gel in the following way

$$m_{p,\infty} \propto A_d \exp(-B_d/f_{gp}) \qquad (71)$$

where $m_{p,\infty}$ is the maximum mobility that the polymer molecules can attain at infinite time under a state of maximum possible disentanglement rate at that
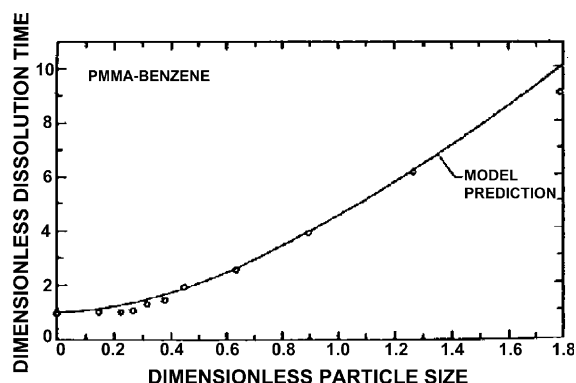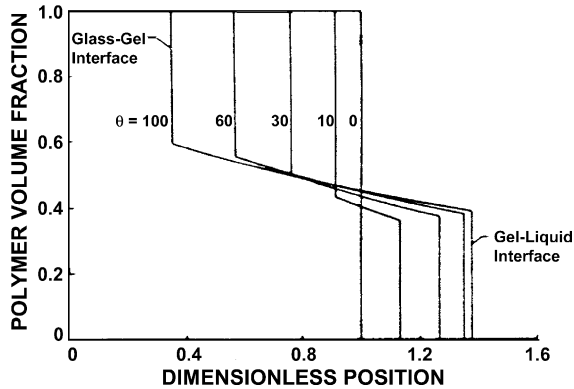
Fig. 15. Polymer concentration profile in the slab for slower glass transition kinetics ($f_{s,t} = 0.15$, $B_d = 1.5$, $f_s^* = 0.3$, $c = 0.35$, $KL_0^2/D_0 = 10^{-7}$). (Adapted from Ref. [86].)

concentration, $B_d$ is a parameter which depends on the size of the mobile species, and $f_{gp}$ is the free volume fraction of the gel phase and is given by

$$f_{gp} = f_{pp}\phi_p + f_{sp}(1 - \phi_p) \tag{72}$$

The concentration at the glassy–gel interface is calculated by using thermodynamics of swollen networks.

Fig. 15 shows the polymer volume fraction profiles as a function of time, produced from simulations. The effect of the parameter $B_d$ on the dissolution kinetics of the polymer is presented in Fig. 16. $B_d$ directly affects the surface disengagement rate. As the size of the mobile molecule increases, the value of $B_d$ gets larger. For high $B_d$ values, the dissolution rate is low and the fraction of the chains disengaged increases continuously with time, and it remains disengagement limited throughout the dissolution process. However,
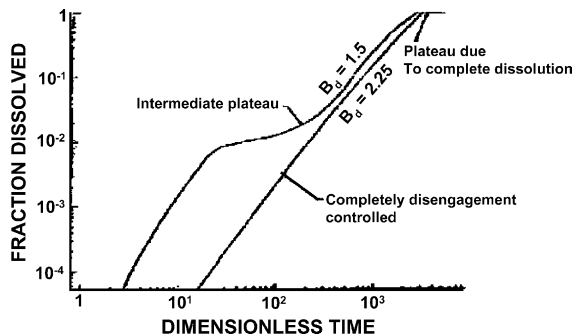


Fig. 16. Effect of the parameter $B_d$ on the dissolution kinetics. $d/L_0 = 0.15$, $D_p/D_s = 10^{-4}$, $f_p^* = 0.4$, $KL_0^2/D_0 = 10^{-7}$, $f_{s,t} = 0.2$. (Adapted from Ref. [86].)
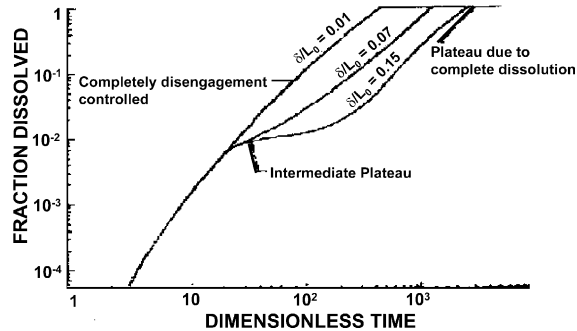


Fig. 17. Effect of thickness of the boundary layer on the dissolution kinetics. $B_d = 1.5$, $d/L_0 = 0.15$, $D_p/D_s = 10^{-4}$, $f_p^* = 0.4$, $KL_0^2/D_0 = 10^{-7}$, $f_{s,t} = 0.2$. (Adapted from Ref. [86].)

as the parameter $B_d$ decreases and the disengagement rate increases, the process is initially disengagement limited and becomes diffusion limited when the diffusion of the chains becomes insufficient to drive away the disengaged chains to the bulk. Therefore, a decrease in the dissolution rate is observed, as observed by the plateau in Fig. 16. The effect of the diffusion boundary layer thickness on the dissolution mechanism is also correct and it was observed that the mechanism shifted from disentanglement-controlled to diffusion-controlled with increased thicknesses (Fig. 17).

### 4.1.3. Dissolution by mixed solvents

Devotta and Mashelkar [88] proposed a model for polymer dissolution in mixed solvents. They assumed that the kinetics of dissolution is completely controlled by the process of disengagement of chains from the gel–liquid interface. The diffusion of the two solvents into the polymer film is described by the following equations

$$\partial\phi_1/\partial t = \partial/\partial x(D_1\ \partial\phi_1/\partial x) + \partial/\partial x(v_s\phi_1) \tag{73}$$

$$\partial\phi_2/\partial t = \partial/\partial x(D_2\ \partial\phi_2/\partial x) + \partial/\partial x(v_s\phi_2) \tag{74}$$

where $v_s$ is the swelling velocity which is related to the diffusion of both the solvents as follows

$$v_s = D_1\ \partial\phi_1/\partial x + D_2\ \partial\phi_2/\partial x \tag{75}$$

The diffusivities of the two solvents are modeled as dependent on their sizes and the free volume of the gel phase, which can be expressed as

$$f_{gp} = f_{pp}\phi_p + f_{1p}\phi_1 + f_{2p}\phi_2 \tag{76}$$

where $f_{gp}$ is the free volume of the gel phase, and $f_{pp}$, $f_{1p}$, and $f_{2p}$ are the free volume fractions of the polymer and the two solvents, respectively. The solvent diffusivities are defined as

$$D_1 = A_{d1} \exp(-B_{d1}/f_{gp}) \tag{77}$$

$$D_2 = A_{d2} \exp(-B_{d2}/f_{gp}) \tag{78}$$

The net rate of movement of the gel–liquid interface is described as follows:

$$dS/dt = D_1(\partial \phi_1/\partial x)|_{x=l} + D_2(\partial \phi_2/\partial x)|_{x=S} - k_d \tag{79}$$

The disengagement part of the model is based on the properties previously outlined in a model proposed by Devotta et al. [85]. The mobility of the chain in the gel phase is assumed to vary according to the following kinetics

$$dm_p/\partial t = K(m_{p,\infty} - m_p) \tag{80}$$

This mobility of the polymer molecules depends on the concentration or the free volume, and hence it is given by

$$m_{p,\infty} = A_d \exp(-B_d/f_{gp}) \tag{81}$$

The variation of the interface concentration of both the solvents with the composition of the dissolution medium is evaluated by assuming a thermodynamic equilibrium at the interface and equating the chemical potentials of each of the solvents in both phases.

The concentration of the entanglements decreases as the matrix swells and the macromolecules disentangle in the gel phase. The rate of change of entanglements is driven by [86]

$$dN_e/dt = K(N_{e,\infty} - N_e) \tag{82}$$

where $N_e$ represents the time dependent number moles of physical entanglements, $N_{e,\infty}$ is the number of moles of entanglement at large times corresponding to the concentrated polymer solution at that concentration and is given by [89]

$$N_{e,\infty} = V_0\rho_p(2\phi_p/M_c - 1/M) \tag{83}$$

Here, $M_c$ is critical molecular weight for entanglement, and $M$ is the molecular weight of the polymer. The solvent and non-solvent concentrations at the gel–liquid interface are predicted using a multi-variable Newton–Raphson method.
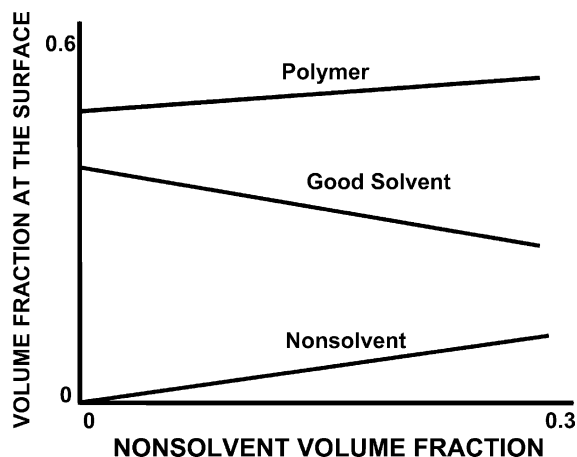


Fig. 18. Predicted variation of initial interface concentration of the two solvents and the polymer with the composition of non-solvent in the dissolution medium. (Adapted from Ref. [88].)

The concentration profiles of the two solvents in the gel phase are obtained from the changing mobility of the chain in the gel phase, and, hence, the disengagement rate can be evaluated.

Fig. 18 shows the general prediction of the variation of surface concentration of both the solvents with the composition of the dissolution medium and the volume fraction of the polymer at the surface, which increases with the non-solvent composition. This indicates lesser swelling of the polymer film with increases in non-solvent content of the solvent phase. The concentration profiles of both the non-solvent and solvent are shown in Figs. 19 and 20, respectively. The concentration profiles for the non-solvent, which
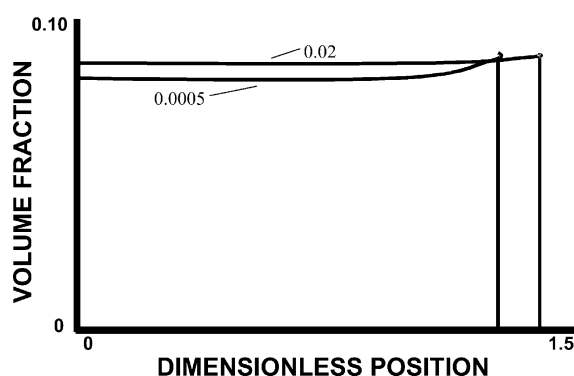


Fig. 19. Concentration profiles of (a) the low molecular size non-solvent and (2) the higher molecular size good solvent in the gel phase. (Adapted from Ref. [88].)
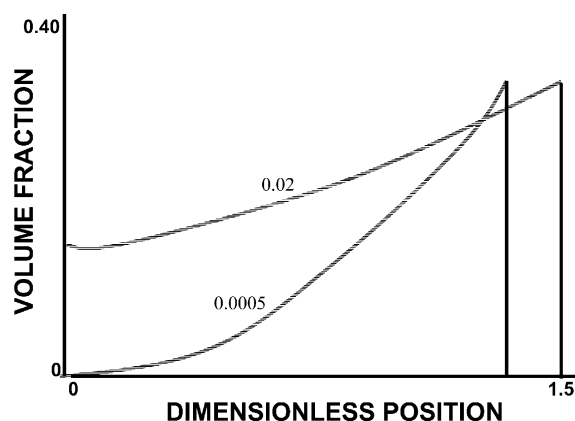
Fig. 20. Predicted variation of normalized dissolution rates with the non-solvent composition in the dissolution medium. (Adapted from Ref. [88].)

diffuses faster than the solvent, are almost flat even at small times, and the concentrations are almost equal to the interface value throughout the matrix. The good solvent diffuses slower because of its larger size. The variation of normalized dissolution rates with the non-solvent composition in the dissolution medium are also predicted. The dissolution rate increases with increased amount of non-solvent due to 'kinetic goodness' of the dissolution medium until a maximum rate is attained. After the maximum, the dissolution rate decreases because the dissolution medium becomes 'thermodynamically poor' resulting in reduced swelling.

### 4.1.4. Drug release from a polymer matrix

Harland et al. [34] developed the first mathematical model for drug release from a polymer matrix during dissolution. It is important to note that when it comes to controlled release systems, they can be classified according to the controlling physical transport mechanisms of drug release, which are diffusion-controlled, swelling-controlled, and chemically controlled. In this model, mass balances are written for the drug and the solvent at the both the glassy–gel and gel–liquid interfaces, and Fickian transport is assumed. When the glassy–gel boundary velocity equals that of the gel–liquid boundary velocity, zero-order release in dissolution-controlled systems occurs. The model was tested with a system of sodium diclofenac from poly(vinyl alcohol) (PVA)-mannitol

tablets, and it yielded good results. However, a disadvantage of this model is that the molecular (or physical) origin of some of the parameters are not available.

Siepmann and co-workers [90–92] formulated a mathematical model describing drug release from dissolving hydroxypropyl methyl cellulose (HPMC) matrices. The dissolved mass of pure HPMC-matrices and the drug release rate from propanolol HCL-loaded HPMC-matrices were determined experimentally. Based on Fick's second law of diffusion for cylinders, the transport of water and drug are modeled considering both radial and axial diffusion, concentration-dependent drug diffusivities, matrix swelling, and HPMC dissolution. The diffusivities of water and the drug are taken to be concentration dependent following a generalized free volume theory, and a reptation model, similar to the approach by Narasimhan and Peppas [93]. The disentanglement processes begin to dominate the dissolution process below a critical polymer concentration, resulting in convection-controlled transport of the polymer chains. This model considered a dissolution rate constant, $k_{diss}$, that characterized the overall dissolution velocity per surface area quantitatively as

$$M_{pt} = M_{p0} - k_{diss} A_t \times t \tag{84}$$

Here, $M_{pt}$ and $M_{p0}$ are the dry matrix masses at time $t$, and $t = 0$, respectively, $A_t$ denotes the surface area of the system at time $t$. The dissolution rate constant $k_{diss}$, was then determined by fitting the model to experimental data (Fig. 21), and it was shown to possess good predictive capabilities. However, the release rates at short and long times are higher and lower than observed, respectively.

### 4.2. External mass transfer arguments

#### 4.2.1. External mass transfer model I

With mass transfer models, the assumption is made that the resistance offered by the layer directly adjacent to the polymer is a controlling factor in polymer dissolution. Lee and Peppas [94] were the first to investigate this phenomenon. The solvent transport is expressed by a Fickian equation

$$\partial \phi_s / \partial t = \partial / \partial x [D_s^v \, \partial \phi_s / \partial x] \tag{85}$$
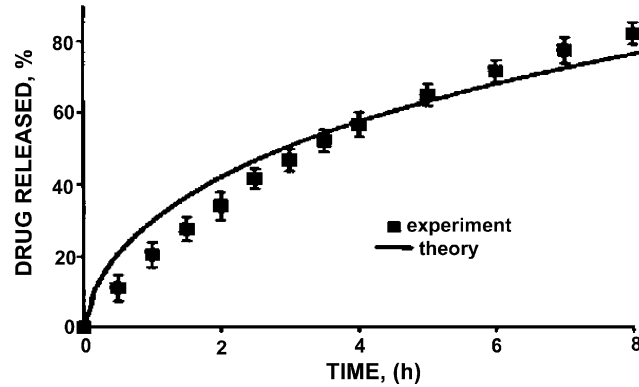
Fig. 21. Validity of the model: predicted and experimentally determined data on propanolol–HCL release from HPMC matrices. (Adapted from Ref. [91].)

where $D_s^v$ is the volume-based diffusion coefficient. The positions of the glass–gel interface, $R$, and gel–liquid interface, $S$, are modeled as

$$-D_s^v\, \partial\phi_s/\partial x = \phi_s\, dR/dt \tag{86}$$

$$-D_s^v\, \partial\phi_s/\partial x - k_p\phi_{p,eq} = (\phi_s + \phi_p)dS/dt \tag{87}$$

The gel layer shows a square-root-of-time dependence and can be calculated by

$$\delta = \{[2tD_s^v(\phi_s^* - \phi_{p,eq}^*)(2 - \phi_s^*)]/[L^2(1 - \phi_s^*)]\}^{1/2} \tag{88}$$

where $\phi_s^*$ is the solvent volume fraction at which the glassy–gel transition occurs and $L$ is the half-thickness of the polymer slab. Experimental data from the literature [83] was compared with the model predictions with good results.

### 4.2.2. External mass transfer model II

Lee and Lee [95] proposed another mass transfer model that also determines the variation of gel thickness with time, in addition to the glassy–gel and gel–liquid boundary positions as a function of time. They also obtained a square-root-of-time dependence of the gel layer thickness like Lee and Peppas [94] and showed that dissolution becomes important only at large experimental times.

### 4.3. Stress relaxation and molecular theories

### 4.3.1. Kinetics of dissolution

Brochard and de Gennes [96] proposed a relaxation-controlled model that relates the solvent flux in the system to the polymer concentration, the stress present in the system and the osmotic pressure. It is assumed that when a droplet of polymer solution with concentration $c_p$ is immersed in a solvent, a two-step process controls the dissolution. The first step involves the solvent swelling the polymer, and the second step corresponds to the viscous yield of the network and is controlled by the reptation time of the polymer, $t_{rep}$. This step is assumed to be controlled by the cooperative diffusion coefficient $D_{coop}$. The net solvent flux is expressed as

$$j_s = K\, \partial/\partial x(\sigma - \pi) \tag{89}$$

where $K$ is a proportionality constant dependent on the polymer concentration, $c_p$, $\sigma$ is the network stress, and $\pi$ is the osmotic pressure. A conservation law is written as

$$\partial c_p/\partial t + \partial j_s/\partial x = 0 \tag{90}$$

The osmotic pressure is expressed as a scaling law with respect to the polymer concentration $c_p$ as

$$\pi \propto c_p^{9/4} \tag{91}$$

and Eq. (88) becomes

$$\partial \pi/\partial t = (9\pi/4c_p)\partial c_p/\partial t = L\, \partial c_p/\partial t \tag{92}$$

where $L$ is a function of $c_p$ (or $\pi$). It was found that for small and large polymer droplets, dissolution was limited by polymer swelling and the viscous yield of the network, respectively. This condition is expressed in terms of a characteristic length, $l$, related to the cooperative diffusion coefficient, $D_{coop}$, and the reptation time, $t_{rep}$ by

$$l = [D_{coop}(c_{p0})t_{rep}(c_{p0})]^{1/2} \qquad (93)$$

They further theorized that for large droplets ($r(0) > 1$), the dissolution is limited by the first step, while for small droplets ($r(0) < 1$), the dissolution is limited by the viscous yield, in addition to the optimal size of droplet of rapid dissolution being $r(0) \sim 1$.

### 4.3.2. The reptation model

Herman and Edwards [97] took the approach of Brochard and de Gennes [96] a step further and examined the stress accompanying the polymer swelling by using reptation theory. Two free energy contributions are included in this model. The first arises from spatial variations in the concentration producing a term in the solvent chemical potential that is proportional to the osmotic pressure $\pi$

$$\mu_s^{OP} = -V_{a,s}\pi \qquad (94)$$

where $\mu_s$ is the chemical potential of the solvent, and $V_{a,s}$ is the average volume of a solvent molecule. OP refers to 'osmotic pressure.' The second contribution arises from the deformation of the polymer due to solvent swelling. This orientational contribution to the chemical potential is evaluated using reptation theory and is given by

$$\mu_s^{OR} = -(V_{a,s}/V_{a,p})\phi_p^2[(dZ/d\phi_p)\Delta G_{seg}^{OR} + Z\partial/\partial\phi_p\Delta G_{seg}^{OR}] \qquad (95)$$

where OR refers to 'orientational', $Z$ is the number of segments in the primitive path and $\Delta G_{seg}^{OR}$ is the orientational contribution to the free energy, given by

$$\Delta G_{seg}^{OR} = k_B T\{-2\ln\Phi - 3 + [3\Phi\cos^{-1}\Phi]/[\sqrt{(1-\Phi^2)}]\} \qquad (96)$$

where $k_B$ is Boltzmann's constant, $\Phi$ is a factor that determines the extent of the local swelling. Fig. 22 shows varying $\mu_s$ behavior resulting from the interplay between the osmotic pressure and orientational stress terms. The parameter $B$ appearing in the figure is given by

$$B = l_m^3/V_m \qquad (97)$$

where $V_m$ and $l_m$ are the monomer volume and length, respectively. It is assumed that the polymer
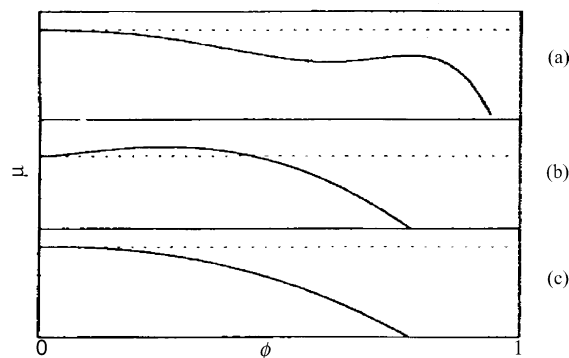


Fig. 22. Solvent chemical potential as a function of polymer volume fraction. (a) $m = 8.0$, $Z_s = 0.1$, $B = 0.064$; (b) $m = 1.0$, $Z_s = 0.05$, $B = 0.26$; (c) $m = 1.0$, $Z_s = 0.01$, $B = 2.6$. The degree of polymerization is 10 000 in each case. The dotted line specifies the zero of the chemical potential. The scale of the chemical potential axis is determined by the choice of the constant $k_B TV_{a,s}/V_{a,p}$. Reprinted with permission from Macromolecules 1990;23(15):3662–71. © 1990 American Chemical Society [97].

volume fraction in the dilute solution phase is low. If this low concentration is established throughout this phase rapidly compared with the time scale of the swelling of the concentrated polymer phase, then the polymer flux across the boundary between the dilute and concentrated phases is negligible. This is incorporated into simple Fickian transport equations with a free volume diffusion coefficient. The flux boundary condition at $x=S$ is written as

$$[-D\,\partial\phi_p\partial x]_{x=S} = \phi_{p,b}\,dS/dt \qquad (98)$$

The transport equations are dimensionless and are solved numerically. Fig. 23 shows a typical polymer volume fraction vs. position profile. It can be seen that $\phi_p$ approaches the bulk value for long times, and the phase boundaries disappear when this happens.

### 4.4. Anomalous transport models and scaling laws

### 4.4.1. Scaling approach

Papanu et al. [89] devised a model of dissolution using scaling laws to model the reptation of a polymer from a swollen gel layer. First, the disentanglement rate, $R_d$, is taken to be proportional to a characteristic length such as the radius or gyration, $r_g$, divided by a characteristic time such as reptation time, $t_{rep}$. Thus,
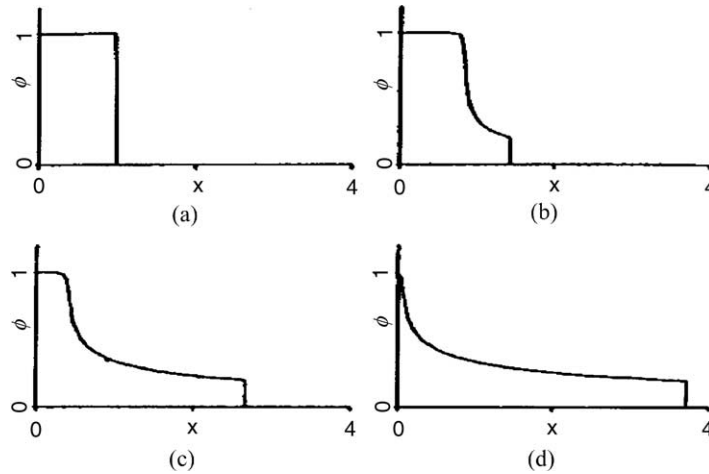
Fig. 23. Polymer volume fraction profiles as a function of dimensionless position at various times. The model parameters are $a_d = 10, f_{p,b} = 0.2$. The dimensionless times are (a) $t = 9.08 \times 10^{-5}$; (b) $t = 4.54 \times 10^{-4}$; (c) $t = 1.36 \times 10^{-3}$; (d) $t = 3.63 \times 10^{-3}$. Reprinted with permission from Macromolecules 1990;23(15):3662–71. © 1990 American Chemical Society [97].

$$R_d \sim r_g/t_{rep} \tag{99}$$

The reptation time constant is expected to be proportional to a length squared divided by the self-diffusion coefficient, $D_{self}$ :

$$t_{rep} \sim r_g^2/D_{self} \tag{100}$$

Combining Eqs. (98) and (99) gives

$$R_d \sim D_{self}/r_g \tag{101}$$

It was shown by de Gennes [98] that

$$r_g \sim M^{0.5}/(1 - \phi_s)^{0.125} \tag{102}$$

and

$$D_{self} \sim 1/M^2(1 - \phi_s)^{1.75} \tag{103}$$

Therefore, the disentanglement rate is expressed as

$$R_d = C/M^{2.5}(1 - \phi_s)^{1.625} \tag{104}$$

where $C$ is an empirical constant.

The kinetics of the glassy–rubbery interface is governed by the stress level as

$$dR/dt = -K(\sigma - \sigma c) \tag{105}$$

where $K$ is a front factor, and $\sigma_c$ is the critical stress for crazing given by

$$\sigma_c = \gamma(T_g - T) \tag{106}$$

where $\gamma$ is a constant and $T_g$ is the glass transition temperature of the polymer.

The movement of the rubbery–solvent interface, $S$, is governed by the difference between the solvent penetration flux and the dissolution rate. An implicit Crank–Nicholson technique with a fixed grid was used to solve the model equations. The positions of the R and S interfaces are shown in Fig. 24, and typical solvent concentration profile is shown in Fig. 25. The solvent concentration at the gel–liquid interface was calculated using the thermodynamics of swollen networks to obtain an equilibrium value at the interface. Typical Case II behavior and disentanglement-controlled dissolution was observed.

### 4.4.2. Dissolution clock approach

Peppas et al. [99] proposed a dissolution model based on chain disentanglement and introduced the idea of a dissolution clock. An expression for the reptation time is derived from the reptation theory and the resultant scaling laws [98,100,101] and it scales as follows [102]

$$t_{rep} \sim L_t^2/D_{tube} \tag{107}$$

where $L_t$ is the length of the tube, and $D_{tube}$ is the tube diffusion coefficient and is expressed as

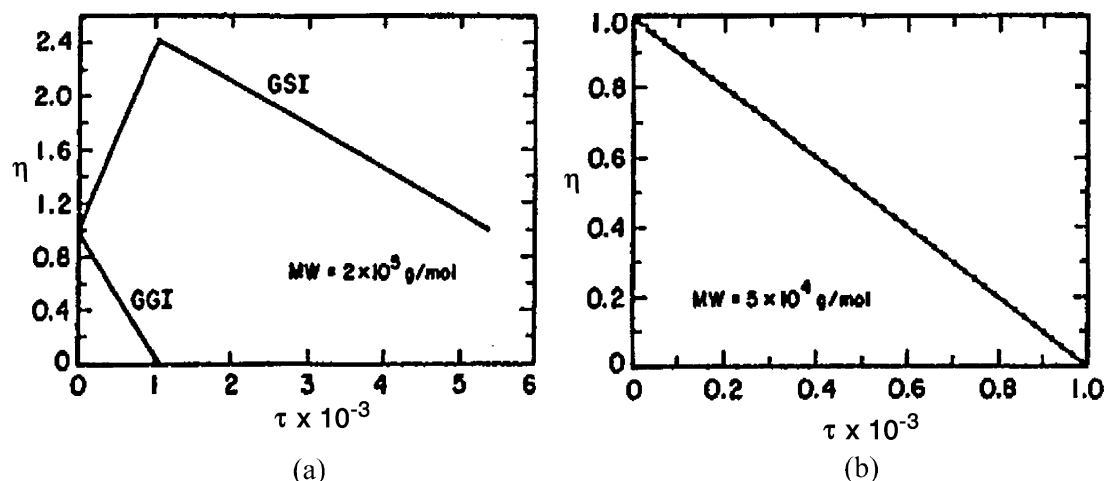$$D_{tube} \sim k_B T m_p \tag{108}$$

Fig. 24. Positions of the glassy–rubbery (R) and the rubbery–solvent (S) interfaces as a function of dimensionless time: (a) corresponding to disentanglement limited dissolution: $M = 20\,000$ and $f_{s,eq} = 0.64$; (b) corresponding to penetration limited dissolution-$M = 50\,000$ and $f_{s,eq} = 0.665$. The position of the rubbery solvent interface is denoted by the filled circles. Parameters for both cases are $L = 10^{-4}$ cm, $K = 9.0 \times 10^{-9}$ cm/(s atm), $s_c = 532$ atm, $V_s = 76.5$ cm$^3$/mol and $T = 323$ K. Reprinted from J Appl Polym Sci 1989;38(5):859–85. © 1989 John Wiley and Sons, Inc. [89].

and, the tube length scales as

$$L_t \sim (M/g)\xi \tag{109}$$

where $\xi$ is the distance between entanglements and $g$ is the number of monomer units in an entanglement subunit.

The radius of gyration is expressed as

$$r_g \sim (M/g)^{0.5}\xi \tag{110}$$

where $g$ becomes

$$g = \phi_p\xi^3 \tag{111}$$

As a result,

$$r_g \sim M^{0.5}\phi_p^{-0.125} \tag{112}$$

The polymer self-diffusion coefficient can be expressed as

$$D_{self} \sim k_BT/\eta_s\xi(g/M)^2 \tag{113}$$

where $\eta_s$ is the solvent viscosity, and, with substitutions, can be rewritten as

$$D_{self} \sim k_BT/\eta_s\xi M^{-2.0}\phi_p^{-1.75} \tag{114}$$

using the expression developed by de Gennes [98]

$$t_d \sim r_g^2/D_{self} \tag{115}$$

where $t_d$ is the disentanglement time and can be rewritten as

$$t_d = K\eta_s/k_BTM^{3.0}\phi_p^{1.5} \tag{116}$$

For good solvents,

$$\xi \sim \phi_p^{-0.75} \tag{117}$$

and

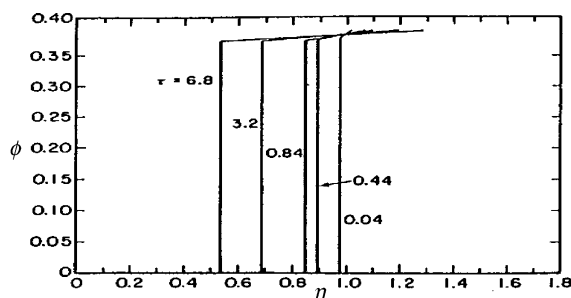$$\chi > 0.5, \qquad \xi \sim \phi_p^{\alpha} \tag{118}$$



Fig. 25. Concentration profiles and boundary locations for Case II swelling at several dimensionless times. $L = 10^{-4}$ cm, $c = 0.876$, $K = 9.0 \times 10^{-9}$ cm(s atm), $(_c = 532$ atm, $V_s = 76.5$ cm$^3$/mol, $D_0 = 10^{-11}$ cm$^2$/s, $M = 200\,000$, $T = 323$ K and $Pe = 1.0$. Reprinted with permission from J Appl Polym Sci 1989;38(5):859–85. © 1989 John Wiley and Sons Inc. [89].

Consequently,

$$t_d = K\eta_s/k_B TM^{3.0}\phi_p^{6\alpha-3} \tag{119}$$

where $K$ is a function of the thermodynamic compatibility between the polymer and the solvent. Thus a general expression for the disentanglement times is written as

$$t_d = k_d M^\alpha \phi_p^\beta \tag{120}$$

Wu and Peppas [103] introduced a numerical algorithm to analyze complex problems of penetrant transport which was extended to model dissolution. The appropriate boundary condition for the gel–liquid interfaces, S, take into account the disentanglement time as defined by Peppas et al. [99]. Thermodynamics of swollen networks are used to estimate the concentration at this interface.

The concept of a dissolution clock was introduced. The clock is initially set to zero at every point within the polymer. When the solvent concentration reaches a critical value, the clock is started, and after a period of time equal to the reptation time, the polymer dissolves. This is clock concept is pictorially shown in Fig. 26.

A system of PS and MEK were tested and the results compared with the model predictions. Fig. 27 shows the predicted movement of $R$ and $S$ with time. From this data, three stages of dissolution are recognized. Further, there is solvent-penetration induced swelling without dissolution. Then dissolution starts after an induction time. Lastly, disentanglement occurs until the polymer completely dissolves.
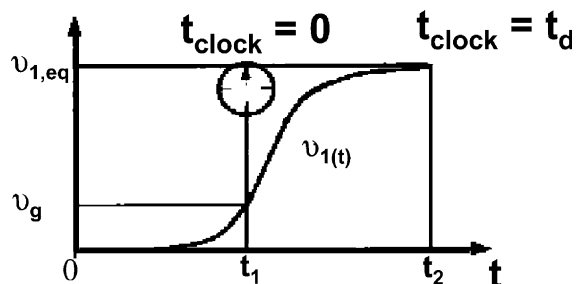


Fig. 26. Solvent volume fraction history at a spatial point. When the solvent volume fraction is equal to the critical gel volume fraction, the dissolution clock starts, $t_1$. When the clock time, $t_2$, is equal to the disentanglement time, $t_d$, the polymer at this point is dissolved. (Adapted from Ref. [99].)
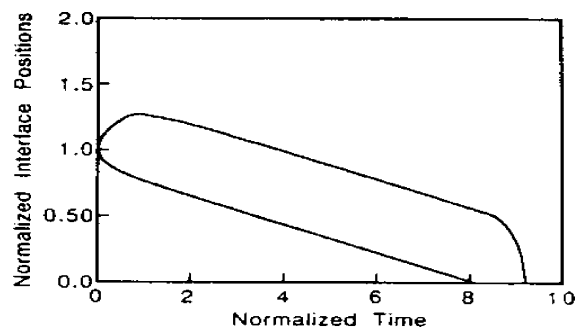


Fig. 27. Numerical predictions of the interface positions normalized with respect to the half-thickness, $L_0$, as functions of dimensionless time during dissolution of PS in MEK. The upper curve represents the solvent–gel interface while the lower curve represents the gel–glass interface position. The parameters used in the simulation were $L_0 = 0.01$ cm, $M = 400\,000$, $M_c = 38\,000$, $c = 0.49$, $D_0 = 1.1 \times 10^{-10}$, $a_d = 20$, $k_d = 2.15 \times 10^{-4}$, $a = 2$, $b = 12$. Reprinted with permission from Macromolecules 1994;27(20):5626–38. © 1994 American Chemical Society [99].

### 4.4.3. The single phase model

Vrentas and Vrentas [104] proposed that for a dissolution process, there are no moving boundaries in the diffusion field. Consequently, the processes of solvent penetration and disentanglement of polymer chains are considered to be part of a complex diffusion process involving polymer and solvent in a single phase. For the dissolution of either rubbery or glassy polymers, the species continuity equation for the polymer is expressed as

$$\partial\rho_p/\partial t + \partial(\rho_p v^\dagger)/\partial x = \partial/\partial x(D\,\partial\rho_p/\partial x) \tag{121}$$

where $v^\dagger$ is the $x$ component of the volume average velocity, and $D$ is the binary mutual diffusion coefficient. Appropriate boundary conditions are defined, the equations converted to dimensionless forms, and Eq. (120) could be rewritten as

$$\partial c_p/\partial\tau = \partial/\partial\lambda(D/D_s\partial c_p/\partial\lambda) \tag{122}$$

Here, $c_p$ is the dimensionless polymer concentration, $\tau$ is the dimensionless time, and $\lambda$ is the dimensionless length scale. This equation is a reasonable approximation to the equation for the dissolution of both glassy and rubbery polymers, and the only difference between dissolution of glassy and rubbery systems in the proposed model is the expected difference in the strength of the concentration dependence of the two cases. An exponential

concentration dependence of the mutual diffusion coefficient is expressed as follows

$$\kappa c_p \geq 0, \qquad D/D_s = \exp(-\kappa c_p) \tag{123}$$

Therefore, the strength of the concentration dependence can be characterized by a ratio, $r$, as follows

$$r = D(c_p = 0)/D(C = 1) = \exp(\kappa) \tag{124}$$

The concentration distribution in the liquid phase can thus be determined for the dissolution of the polymer. Dissolution curves are constructed by plotting the fraction of polymer which dissolves versus the square root of dimensionless time (Fig. 28). The dissolution curves are linear in the early stages of dissolution. For $r = 1$ and 10, the slopes of the curves decrease with increasing times, but for sufficiently high values of $r$, it becomes evident that there is an increase in the slopes before the dissolution curves eventfully flatten to the value of unity. As a result, it appears that the dissolution curves assume sigmoidal shapes for sufficiently high values of $r$. It was concluded that the dissolution process was only moderately sensitive to the strength of the concentration dependence of the mutual diffusion coefficient. The dimensionless time when the fraction dissolves is equal to 1/2, the half-time for dissolution.

Even though it is assumed that the dissolution process involves only one phase with no interfaces, it is possible to suppose that pseudointerfaces exist at certain dimensionless polymer concentrations.
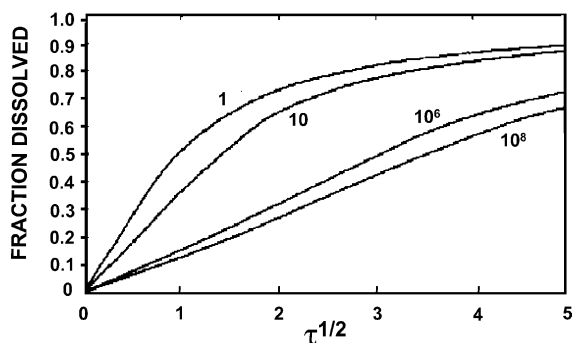


Fig. 28. Dissolution curves for four values of $r$, the diffusivity ratio defined by Eq. (124). (Adapted from Ref. [104].)
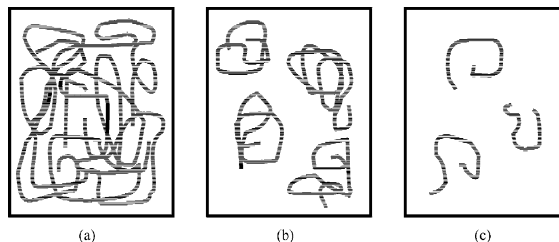


Fig. 29. Disentanglement of polymer chains (a) before dissolution starts, there is no disentanglement; this is a swellable system. (b) This depicts the onset of dissolution in the diffusion boundary layer. (c) The dissolution is complete and the disentangled chains exhibit Brownian motion in the solvent. (Adapted from Ref. [104].)

## 4.5. Molecular theories in a continuum framework

### 4.5.1. Dissolution of a rubbery polymer

Narasimhan and Peppas [105] analyzed the dissolution mechanism of rubbery polymers by dividing the penetrant concentration field into three regimes that delineated three distinctly different transport processes (Fig. 29). The first regime consists of the swollen rubber and is deemed the 'concentrated' regime. The existence of a diffusion boundary layer adjacent to the rubber–liquid interface, $S$, is defined as the 'semi-dilute' regime. The 'dilute' regime is defined when the polymer is fully dissolved and the disentangled chains move freely in the solvent, exhibiting Brownian motion.

Because the solvent transport through rubbery polymers is generally known to be Fickian, the solvent penetration is presented as

$$\partial \phi_s/\partial t = \partial/\partial x(D \, \partial \phi_s/\partial x) \tag{125}$$

Appropriate boundary conditions are defined.

As the macromolecules disentangle, they move out of the gel-like phase to a liquid solution through a diffusion boundary layer of thickness, $\delta$, which is assumed to be constant. The chain transport through this boundary layer is described as

$$\partial \phi_p/\partial t = \partial/\partial x(D_p \, \partial \phi_p/\partial x) - dS/dt \, \partial \phi_p/\partial x \tag{126}$$

This equation is valid in the region between $x = S$ and $x = S + \delta$, and the initial boundary conditions are

$$t = 0, \qquad \phi_p = 0 \tag{127}$$

At the end of the boundary layer, the conventional boundary condition is

$$x - S(t) + \delta, \ \phi_p = 0 \tag{128}$$

The boundary condition on the solvent side of the rubber–liquid interface is written by considering that a polymer chain requires a minimum time to disentangle and move out of the gel. This minimum time is the reptation time, $t_{rep}$. Hence, the disentanglement rate is zero until a time equal to the reptation time elapses:

$$-D_p \ \partial\phi_p/\partial x = 0, \qquad x = S^+(t),$$
$$0 < t < t_{rep} - D_p \ \partial\phi_p/\partial x = 0 \tag{129}$$

After the reptation time is complete, the transport of the chains at the rubber–liquid interface may be disentanglement-limited or diffusion-limited. The rate of diffusion is sufficiently high at times just greater than $t_{rep}$, so the flux is disentanglement-limited. Therefore, the boundary condition was written as

$$-D_p \ \partial\phi_p/\partial x = k_d, \qquad x = S^+(t), \ t < t_{rep} \tag{130}$$

The polymer concentration in the boundary layer eventually reaches an equilibrium value, $\phi_{p,eq}$, and the diffusion rate becomes insufficient to transport the chains, at which point this polymer concentration is maintained. It was proposed that an equilibrium exists between the polymer-rich gel and the polymer-lean solvent in the diffusion boundary layer, and the boundary condition becomes

$$x = S^+(t), \qquad \phi_p^+ = \phi_{p,eq}, \ t < t_{rep} \tag{131}$$

As the solvent swells the polymer, the rubber–liquid interface $S$ moves and this is expressed as

$$dS/dt = (D \ \partial\phi_p/\partial x)^- - D_p/\phi_s^- \ (\partial\phi_p/\partial x)_+, \ S(0) = 1 \tag{132}$$

It is shown that there exists a critical solvent concentration $\phi_{s,c}$, at which the diffusivity of the system changes as follows

$$D = D_s, \qquad \phi_s < \phi_{s,c} \tag{133}$$

$$D = D_p, \qquad \phi_s > \phi_{s,c} \tag{134}$$

where

$$D_s = D_{s,0} \exp(a_d \phi_s) \tag{135}$$

and $D_{s,0}$ is the diffusivity of the solvent in a glassy polymer and $D_p$ is a 'reptation' diffusion coefficient.

It is postulated that for a dissolving polymer, the disentanglement rate, $k_d$, is the ratio of the radius of gyration $r_g$, to the reptation time, $t_{rep}$ :

$$k_d = r_g/t_{rep} \tag{136}$$

This assumption is made based on previous work [98,102] showing that a polymer requires a time equivalent to its reptation time to disentangle and that the distance that the chain travels during that time can be approximated by its radius of gyration.

The model was tested and typical profiles for the solvent volume fraction as a function of position and time in the rubber and the polymer volume fraction in the diffusion boundary layer are shown in Figs. 30 and 31. Other features of the simulation are the prediction of the temporal evolution of the rubber–solvent interface and the mass fraction of the polymer dissolved as a function of time (Figs. 32 and 33). The simulations showed that the dissolution is either disentanglement- or diffusion-controlled depending on the polymer molecular weight and the thickness of the diffusion boundary layer.

### 4.5.2. Dissolution of a glassy polymer

Narasimhan and Peppas [106] extended their previous dissolution model for rubbery polymers
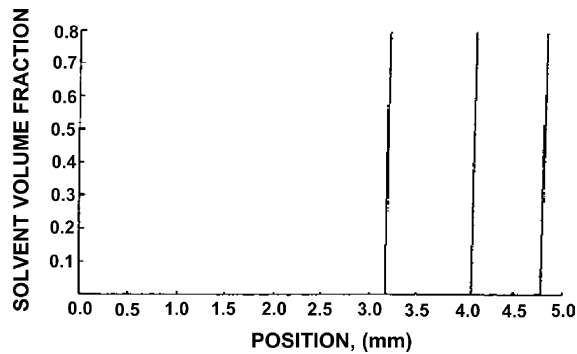


Fig. 30. Solvent volume fraction, $f_s$ as a function of position, $x$. The polymer molecular weight was $M = 40\,000$ and $t_{rep} = 1000$ s. The position $x = 0$ is the center of the slab. The time increment starting from the first curve on the right is $D_t = 1000$ s. (Adapted from Ref. [105].)
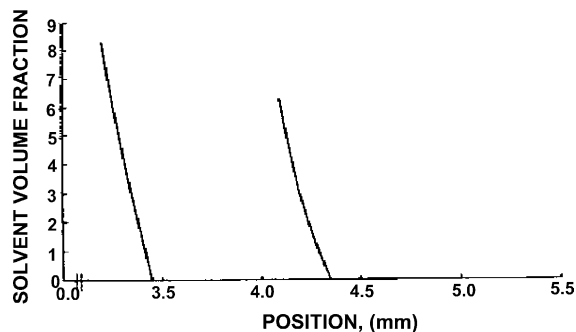
Fig. 31. Polymer volume fraction, $f_s$, in the diffusion boundary layer, as a function of position, $s$. The polymer molecular weight was $M = 40\,000$ and $t_{rep} = 1000$ s. The position $x = 5$ mm represents the initial slab thickness. The time increment starting from the first curve on the right is $D_t = 1000$ s. (Adapted from Ref. [105].)

[105] to interpret glassy polymers. Much of the theory and assumptions in this model are the same as that of the rubbery polymers, however, the concentrated regime consists of the region of polymer that has undergone a glass-to-rubber transition due to solvent penetration.

The solvent flux is expressed as a sum of contributions from diffusive and osmotic pressure terms as follows:

$$\phi_s v_s = -\,[D\,\partial\phi_s/\partial x + DV_{s,s}\phi_s/RT(1 - \phi_s)$$
$$\times (1 - 2\chi_{sp}\phi_s)\partial\pi/\partial x] \tag{137}$$

where $v_s$ is the velocity of the solvent in the $x$ direction, $V_{s,s}$ is the specific volume of the solvent, $\chi_{sp}$ is the solvent–polymer interaction parameter, and $\pi$ is osmotic pressure, which depends upon the
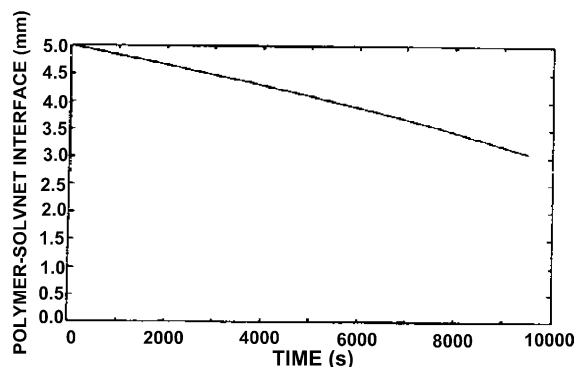


Fig. 32. The position of the rubbery–solvent interface, $S$, as a function of dissolution time The polymer molecular weight was $M = 40\,000$ and $t_{rep} = 1000$ s. (Adapted from Ref. [105].)



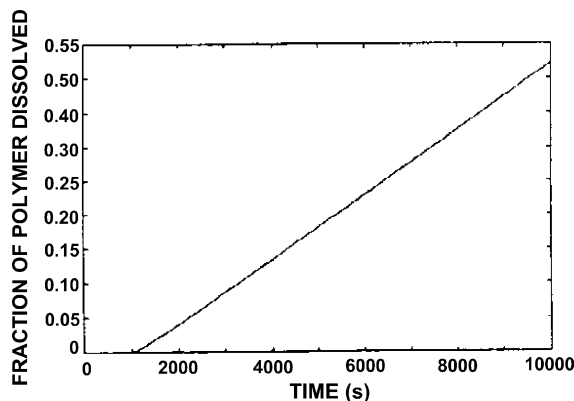Fig. 33. The fraction of polymer dissolved as a function of time. The polymer molecular weight was $M = 40\,000$ and $t_{rep} = 1000$ s. (Adapted from Ref. [105].)

viscoelastic properties of the polymer. Momentum balances are used to relate the osmotic pressure to the stress existent within the polymer and derived the relationship

$$\partial\pi/\partial x = \partial\sigma_{xx}/\partial x \tag{138}$$

where $\sigma_{xx}$ is the normal stress. A Maxwell model was used to express the viscoelastic behavior of the polymer and the governing equations for the concentrated regime were obtained as

$$\partial\phi_s/\partial t = \partial/\partial x[D\,\partial\phi_s/\partial x] + \partial/\partial x[DV_{s,s}\phi_s/RT(1 - \phi_s)$$
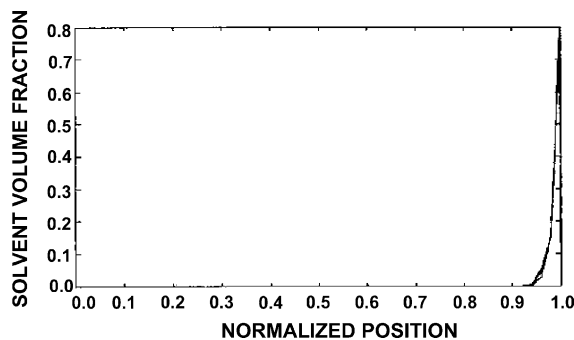$$\times (1 - 2\chi_{sp}\phi_s)\partial\sigma/\partial x] \tag{139}$$



Fig. 34. Solvent (MEK) volume fraction, $f_s$, as a function of normalized position. The PS molecular weight $M = 52\,000$. The position $= 0$ is the center of the slab. The time increment starting from the first curve on the right is $D_t = 1000$ s. (Adapted from Ref. [106].)
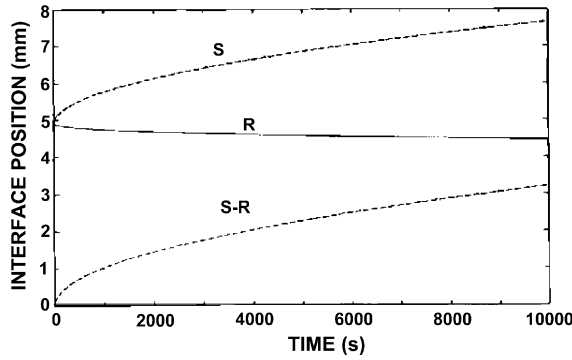
Fig. 35. Rubbery–solvent interface (S), glassy–rubbery interface (R), and gel layer thickness (S–R) as a function of normalized position. The PS molecular weight $M = 52\,000$. (Adapted from Ref. [106].)

$$\partial \sigma_{xx}/\partial t = -\sigma_{xx}/(\eta/E) + E/(1 - \phi_s)^2 \partial \phi_s/\partial t \qquad (140)$$

where $\eta$ is viscosity, and $E$ is the spring modulus.

A mathematical simulation of the model was tested using a system consisting of PS dissolving in MEK. Fig. 34 shows the solvent volume fraction in the polymer as a function of time and position. The position of the interfaces R and S as a function of time are shown in Fig. 35. Integrating the concentration profiles, the mass fraction of polymer dissolved as a function of time was obtained (Fig. 36). Upon increasing the polymer molecular weight, the dissolution became disentanglement-controlled, but decreasing the diffusion boundary layer thickness shifted the dissolution mechanism to diffusion-controlled.
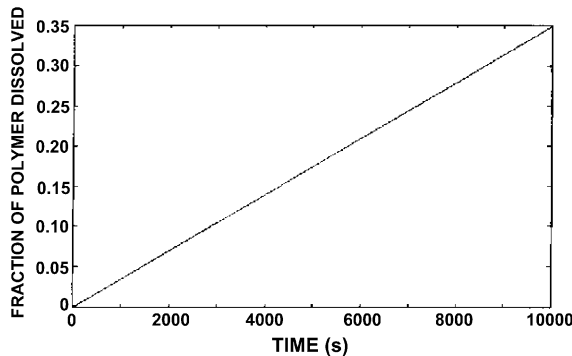


Fig. 36. Fraction of PS dissolved as a function of time. The PS molecular weight $M = 52\,000$. (Adapted from Ref. [106].)

### 4.5.3. Molecular model for drug release I

Narasimhan and Peppas modified the phenomenological drug delivery model developed by Harland et al. [34] by applying their models [105,106] and incorporating the macromolecular chain disentanglement. A three-component system is considered, with water as component 1, the polymer as component 2, and the drug component 3. The model considers the two moving boundaries, $R$ and $S$, previously discussed in their models for rubbery and glassy polymer dissolutions. Quasiequilibrium conditions at the rubbery–solvent interface enable the use of the Flory–Rehneer theory [106] to calculate the water and drug volume fractions at this interface. The variation of the gel layer thickness (S–R) with time is obtained as

$$-(S-R)/B_C - (A_C/B_C^2)\ln[1 - (B_C/A_C)(S-R)] = t \qquad (141)$$

where

$$A_C = D_S(\phi_{s,eq} - \phi_{sc})[\phi_{s,eq}/\phi_{s,eq} + \phi_{d,eq}$$
$$+ 1/(\phi_{sc} + \phi_{dc})] + D_d(\phi_{dc} - \phi_{d,eq})$$
$$\times [\phi_{d,eq}/(\phi_{s,eq} + \phi_{d,eq}) + 1/(\phi_{sc} + \phi_{dc})] \quad (142)$$

$$B_C = k_d/(\phi_{s,eq} + \phi_{d,eq}) \qquad (143)$$

and an expression for the fraction of the drug released is derived as

$$M_d/M_{d,\infty} = (\phi_{d,eq} + \phi_{dc})/2l((2A_Ct)^{1/2} + B_Ct \qquad (144)$$

where l is the half-thickness of the polymer, $\phi_{sc}$ and $\phi_{dc}$ are characteristic concentrations of solvent and drug, respectively, $\phi_{s,eq}$ and $\phi_{d,eq}$ are equilibrium concentrations of solvent and drug, respectively, $k_d$ is the disentanglement rate of the polymer chains. Fig. 37 shows the predicted normalized gel layer thickness as a function of normalized time for different values of $A_C/B_C$. As $A_C/B_C$ approaches zero, the gel layer thickness profile becomes flat (disentanglement-controlled) while for higher values of $A_C/B_C$, then it increases with time (diffusion-controlled). Model predictions were compared with experimental results [93,107] and were in good agreement.
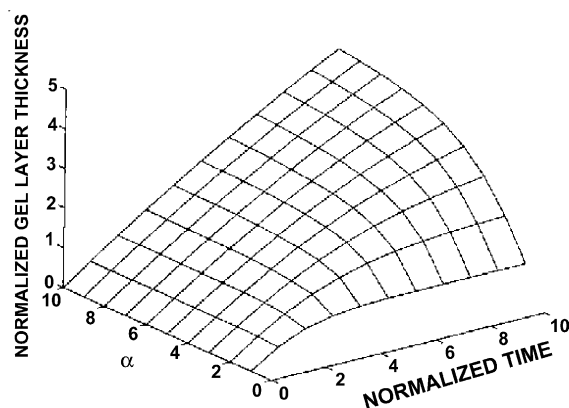
Fig. 37. Predicted normalized gel layer thickness, $d/l$ as a function of normalized time, $t$, for different values of $A_C/B_C$. (Adapted from Ref. [93].)

### 4.5.4. Molecular model for drug release II

Ju et al. [108–110] proposed a mathematical model of drug release from hydrophilic matrices based on the diffusion layer and a polymer disentanglement concentration, $\rho_{p,dis}$, which is defined as the concentration below which the chains detach from the matrix and diffuse through the diffusion layer into the bulk solution and scaled as

$$\rho_{p,dis} \sim M^{-0.8} \tag{145}$$

The mathematical description of the transport accounts for swelling/dissolution in the radial direction and also derives 'universal' scaling relationships for the fraction release of both polymer and drug with respect to the polymer molecular weight, $M$. A weaker molecular weight dependence for the drug is predicted, and, for very large values of $M$, both fractional release profiles approach limiting values. These results agree well with experimental data on fractional release of HPMC and adinazolam mesylate form HPMC matrices of various molecular weights.

Ju et al. also developed a model for the diffusion coefficients of disentangled HPMC chains in the diffusion layer adjacent to the matrix [110]. They showed that the effective diffusion coefficient scales with $M$ as

$$D_{eff} \sim M^{-0.53} \tag{146}$$

and the chains exhibit Zimm dynamics [111] within the diffusion layer regime, providing a scaling

relationship of

$$D_{Zimm} \sim M^{-0.5} \tag{147}$$

which is very close to the result that they derived.

## 5. Techniques used to study polymer dissolution

Various experimental techniques have been utilized to characterize polymer dissolution behavior. Some of these techniques include differential refractometry, optical microscopy, fluorescence, gravimetry, interferometry, NMR, and FT-IR imaging. This section describes these techniques and how they are used to monitor polymer dissolution. The advantages and disadvantages of the methods are also be discussed.

### 5.1. Differential refractometry

One of the earliest techniques used to study polymer dissolution was refractometry [12]. The basis of this technique is that during the dissolution process, the polymer concentration increases continuously in the solvent, and this concentration can be measured by the refractive index. While this technique provides some measurements of the dissolution process and detects small changes in polymer concentration in the solvent phase, no information can be obtained about the surface layer of the polymer pellet. Also, when a relatively small amount of polymer is being dissolved in very large quantities of solvent, this method is less satisfactory than when larger quantities of polymer are being dissolved.

### 5.2. Optical microscopy

Optical microscopy allows direct visual observation of the dissolution process and the formation of a gel layer. Therefore, it provides information about the structures of the different layers (solvent, gel, and polymer layers) formed, which can govern the dissolution process. The apparatus used consists of a microscope and a sample cell composed of a slice of polymer pellet encapsulated in a matrix inert to the solvent, which is then sandwiched between two glass slides (Fig. 38). In cases where both the solvent and
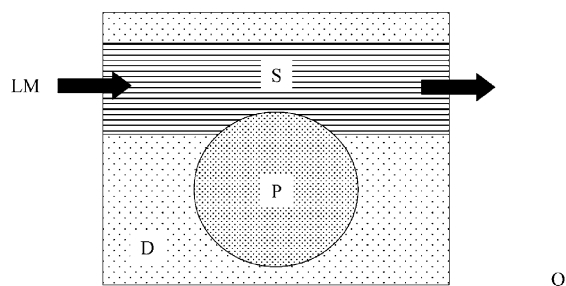
Fig. 38. Interior of microscope thermostat, *P*, polymer sample; *O* and *D*, glass slides; LM, solvent; *S*, channel. (Adapted from Ref. [12].)

the polymer are transparent, it is necessary to use either a dye in the solvent or carbon black in the polymer to track both the penetration of the solvent into the polymer matrix and the dissolution of the swollen polymer in the solvent.

Ouano and Carothers [25] used critical angle illumination microscopy to study in situ dissolution dynamics. They designed an apparatus similar to that of Ueberreiter's, but made major modifications in the sample cell and the optical design which eliminated the need for dye or carbon black tracer. Good contrast between the different layers of the dissolving polymer could be achieved by changing the angle of illumination of the sample, relative to that of the microscope objective. The optimum angle of illumination depended on the refractive indices of both the solvent and the polymer. The sample cell mount was altered to allow greater precision in measuring the motions of the boundaries of the different layers, and the cell design changed to improve flow rate control. With these modifications, direct observations and quantitative measurements became possible.

The use of optical microscopy has provided valuable insight into the behavior of polymers in contact with solvents, but it is limited to a micrometer scale. Additionally, there is limited chemical specificity with an optical microscopic system.

### 5.3. Interferometry

Interferometry has been used to monitor polymer dissolution. The polymer material is placed between two mirror slides. From the number of interference lines produced by a beam of monochromatic light which passes through the swollen layer normal to

the surface, the concentration gradient within the surface layer can be calculated and the velocity of penetration deduced by observing the position of the retracting front of the polymer at successive times on a micrometer scale.

Laser interferometry is a popular method of dissolution rate measurements by the microelectronics industry. It can also provide quantitative information on the thickness of the transition layer between the dissolving polymer and liquid solvent. Rodriguez and co-workers [15,16,18,30,31] studied polymer dissolution for microlithography applications extensively. The basic apparatus is shown in Fig. 39. A substrate with a very thin ($0.5-1.5$ µm) polymer film is suspended in a transparent cylindrical container filled with a selected liquid. A beam of unpolarized light of wavelength 6328 Å from a 2 mW He–Ne laser is directed obliquely at the film-coated substrate, and the angle of incidence is typically 10°. The reflected beam is collected by a silicon photocell and the recorded signal represents the reflected intensity as a function of time. Reflected light from the substrate–film and film–solvent interfaces produces a pattern of constructive and destructive interference. The periodicity of the interference can then be related to the absolute film thickness at any given time. An advantage of this technique is the ability to delineate the distinct regions with the surface layer of the dissolving polymer. However, there are some disadvantages. First, only transparent films can be monitored. Second, it does not provide direct detailed information about the shape of the concentration profile in the transition layer. Also, problems can occur when the film has a non-uniform surface. This causes light to be scattered, resulting is noisy data that is difficult to interpret.
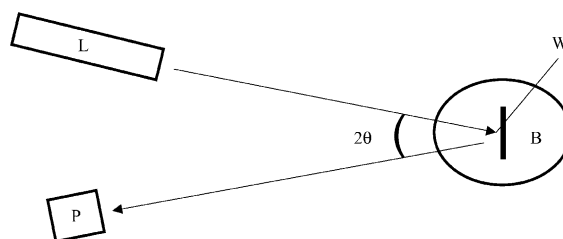


Fig. 39. Interferometer for monitoring polymer dissolution. Beam from laser, *L*, is reflected at angle *θ* from coated wafer, *W*, immersed in solvent bath, *B*. Reflected light is measured with photocell, *P*. (Adapted from Ref. [16].)
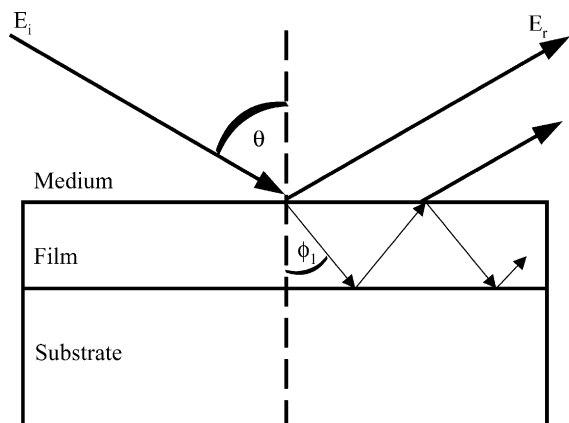
Fig. 40. Incident and reflected light for a single film on a substrate. Only the first two reflected rays are shown. The angle of incidence and the refraction angle in the film are denoted by $\theta$ and $\phi_1$, respectively. (Adapted from Ref. [111].)

## 5.4. Ellipsometry

Ellipsometry is another optical tool used to study polymer dissolution. The basics of ellipsometric measurements were explained by Papanu et al. [112] with the aid of Fig. 40. A light beam incident on a film-covered substrate undergoes reflection and refraction at each interface, leading to the multiple reflections depicted in the figure. The resultant beam is the infinite summation of these multiple reflections. The electric fields of the incident and reflected light beams are described by the complex amplitude $E_i$ and $E_r$. These components can be resolved into two components parallel ($\parallel$) and perpendicular ($\perp$) to the plane of incidence, where the plane of incidence is defined by the incident and reflected beams. The overall reflection coefficients are defined as

$$r_c^{\parallel} = E_r^{\parallel}/E_{i,}^{\parallel} \tag{148}$$

$$r_c^{\perp} = E_r^{\perp}/E_i^{\perp} \tag{149}$$

and the ratio of these two coefficients gives the fundamental equation of ellipsometry

$$\rho = r_c^{\parallel}/r_c^{\perp} = \tan(\psi)\exp(i\Delta) \tag{150}$$

The two parameters $\Delta$ and $\psi$ relate to the relative phase and amplitude change upon reflection, respectively, and can be used to determine thickness and refractive index of the film and vice versa.
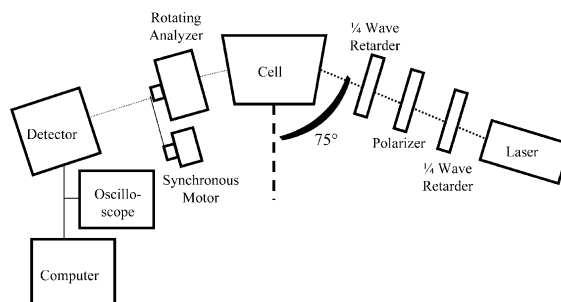


Fig. 41. Schematic of a rotating-analyzer ellipsometer. (Adapted from Ref. [111].)

Papanu et al. [19–21,31,112] have used this technique with good results. A schematic of a rotating-analyzer ellipsometer is shown in Fig. 41. Papanu et al. monitored dissolution in situ with a psi-meter, a single-element rotating-polarizer ellipsomenter in which an incident laser beam is polarization modulated and the intensity fluctuation of the reflected light is measured. The ratio of the AC and DC components of the reflected intensity is related to the optical parameter psi $\psi$ by AC/DC = $-\cos 2\psi$. To determine film thickness as a function of time, calculated values of $\psi$ or AC/DC are compared to experimental data. This is produced using an ellipso-metry software program [113] which gives theoretical values of $\psi$ vs. thickness when the wavelength, angle of incidence, and refractive indexes of the substrate, film and immersion medium are known. Ellipsometry can be used to distinguish between swelling and dissolution, to measure swelling and dissolution rates, differentiate Fickian and Case II diffusion mechanisms, and determine the extent of swelling at equilibrium. Some disadvantages of this technique are that an a priori knowledge of the refractive index of the material is necessary, precision can be limited by detector instability, and accuracy can be limited by uncertainties in analyzer azimuth and angle of incidence.

Limm et al. [114] modified the interferometric technique and studied the dissolution of fluorescence labeled polymer films. In this method, the polymer is labeled with a small amount of fluorescent dye whose fluorescence is quenched by the solvent used to dissolve the film. When the film is exposed to solvent, fluorescence from the dye decreases with time. Loss of fluorescence is due to two effects: (1) diffusion of
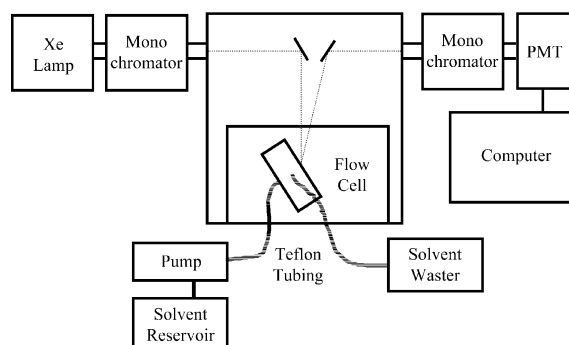
Fig. 42. Schematic of the experimental setup to monitor fluorescence intensity of a polymer film mounted in the flow cell. (Adapted from Ref. [113].)



Fig. 43. Schematic of the quartz crystal microbalance dissolution rate monitor. (Adapted from Ref. [115].)

the solvent molecules into the film which leads to fluorescence quenching and (2) dissolution of the polymer. By monitoring the intensity of fluorescence from the film along with the interferometric signal, the solvent penetration rate into the film and the film dissolution rate are measured simultaneously. Fluorescence intensities are measured with a spectrometer. A schematic of the optical arrangement of a spectrometer is seen in Fig. 42.

### 5.5. Steady-state fluorescence

Pekcan et al. [17,23,24,115] used a steady-state fluorescence (SSF) technique to study dissolution of dissolution and swelling of polymer films in real time. Swelling experiments were carried out by illuminating only the polymer film, so that unquenched pyrene molecules were monitored in real time. Dissolution experiments were designed so that pyrene molecules, desorbing from swollen gel, were detected in real time monitoring of SSF intensity. In order to do this, direct illumination of the film sample was avoided. Measurements of energy transfer during dissolution experiments were performed with a specrofluori-meter, and fluorescence emission intensity was monitored. This technique gave information about effects of stirring, annealing, temperature, polymer molecular weight and solvent quality as well as the second and last steps of polymer dissolution. Diffusion coefficients and relaxation constants of polymer chains were also measured.
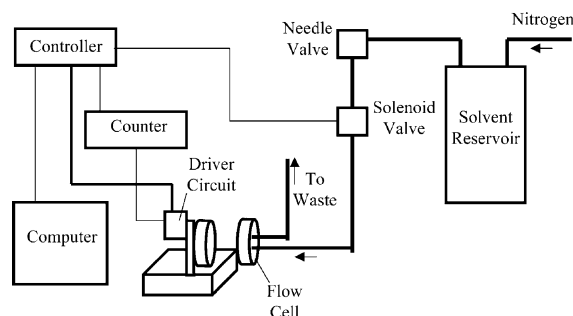
### 5.6. Gravimetry

An alternative to optical techniques is the measurement of film mass during dissolution. This can be accomplished with the use of a piezoelectric quartz crystals, which are fabricated to posses a known oscillation frequency at room temperature. Dissolution measurements can be made using a quartz crystal microbalance (QCM) (Fig. 43). Deposition of a polymer films on a quartz crystal causes it to resonate at a lower frequency than the base frequency of the uncoated crystal. As the film dissolves and the mass decreases, the frequency will rise until the base frequency of the crystal is reached. The change in frequency can then be subsequently correlated with the film thickness through density, substrate area and instrument parameters [116]. The main advantage of this system is that highly accurate frequency measurements can be made. In addition, if surface roughening occurs the quality of the rate data obtained is not compromised as would be the case for an optical technique. However, a disadvantage is that variable viscoelastic properties that polymers exhibit can cause a distortion of the measured oscillation frequency and an inaccurate thickness determination.

### 5.7. Nuclear magnetic resonance (NMR)

Devotta et al. [86] utilized an in situ NMR technique to study dissolution. They showed that NMR was a valuable tool to monitor the molecular level events that take place during the swelling and dissolution of macromolecules. Local molecular changes of environments yield changes in NMR spectral and relaxation behavior. Dynamical events

can be followed by simple line width measurements [117]. The temporal response can be carried out in situ, and this is shown to be related to the microscopic behavior of the chain in response to the macroscopic perturbation (by solvent) through the enhanced molecular mobilities that extend to narrow the otherwise broad proton resonance line. Devotta et al. used the change in the proton line width as a direct measure of the local mobility in a swelling–dissolving system, since this change emits from a spatial averaging of local spin interactions by polymer motions.

Devotta et al. [86] also measured the integrated proton signal area as a function of time to examine the time variation of the population of the dissolved polymeric molecules in the swelling–dissolving polymer. The rationale behind this method was that at temperatures below the glass transition temperature, in the absence of any solvent, the mobility of the polymer is restricted, resulting in a broad proton resonance line. However, as the solvent penetrates into the polymer matrix, the polymer swells and the chains disengage from the swollen surface. The local mobility of the polymer segments in the solvent phase increases appreciably, resulting in the observation of narrower proton signals. Therefore, a direct linear relationship should exist between the integrated signal area and the population of the dissolved polymer in the NMR intensity measurement.

Spin echo NMR has also been applied [32,99]. As the $T_1$ values decrease when the molecular motion becomes faster or when the correlation time decreases. Therefore, the duration of the gradient pulses can be changed sequentially and the spin-echo intensity recorded.

NMR imaging offers a convenient way to obtain both qualitative and quantitative data about the dissolution of macromolecules. By systematically increasing the evolution time and the detection period, a two-dimensional signal is obtained that, when put through a Fourier Transform operation, yields a two-dimensional image replete with spectral data [118]. There are several advantages to this technique [119]. First, it is non-invasive, and it is possible to conduct experiments in situ, depending on the system under study. Also, several chemical-selective techniques exist such that specific species in a system can be selectively imaged. Lastly, the liquid distribution in

any region of a system can be spatially resolves, and the technique is not limited by sample geometry. However limitations do exist. For example, the spin–spin ($T_2$) and spin–lattice ($T_1$) relaxation processes that characterize the return of the spin system to equilibrium following perturbation by radio frequency pulse, can cause attenuation of the NMR signal. To avoid the attenuation of signal intensity by NMR relaxation contrast, Weisenberger and Koenig [118] specified three requirements for the accurate use of NMR imaging of liquids in polymer when using spin-echo imaging techniques as follows: (1) the echo time of the experiment must be less than 10% of the shortest $T_2$ of the system, (2) the recycle time of the experiment must be at least five times longer than the longest $T_1$ of the system, and (3) the experiment time must be less than the time of the inverse of the front velocity.

## 5.8. FT-IR imaging

Koenig et al. have extensively researched polymer dissolution with FT-IR imaging [120–129]. By coupling a step-scan interferometer with an FT-IR spectrometer and a focal plane array (FPA) detector, spatial and spectral information may be collected simultaneously (Fig. 44). The ability of FT-IR to measure the behavior of multiple components within a system simultaneously, when coupled with the spatial resolution of an FPA provides a unique opportunity for observing the dissolution process. With this experimental setup, the behavior of multiple components diffusing into a polymer matrix may be observed. The behavior of binary solutions diffusing into a polymer has been characterized [121–124,
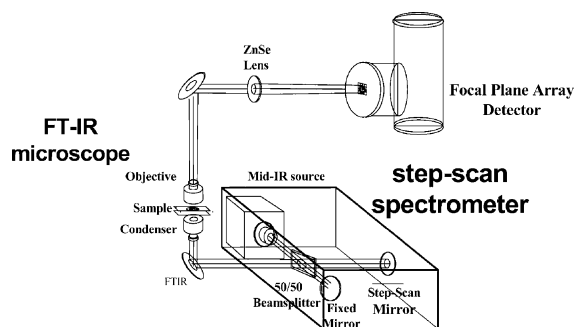


Fig. 44. Schematic of FT-IR imaging set-up.

126–128]. A single experiment yields data on all components in the system, allowing for real-time analysis of both the dissolution process and the behavior of each component within the system.

To measure dissolution, a spectral profile may be taken across the sample, noting the intensity of polymer- or solvent-specific bands across the interface. From these profiles, the behavior of the system may be characterized quickly and easily. The spatial resolution of these images is about 6 μm. Because no apertures are used, the diffraction effects that usually affect resolution do not come into play using this method.

## 6. Conclusions

Polymer dissolution in solvents has been long recognized as an important phenomenon in field ranging form microlithography to tissue engineering. The dissolution of a polymer into a solvent involves two transport processes, namely solvent diffusion and chain disentanglement. Several models have been proposed in effort to understand the physics of the dissolution mechanism of glassy polymers. The approaches to model dissolution of amorphous polymers can be categorized as: (1) phenomenological, (2) external mass transfer, (3) stress relaxation and molecular theories, (4) anomalous transport models and scaling laws, and (5) molecular theories in a continuum framework. These various approaches have incorporated phenomena such as stress relaxation, polymer viscoelasticity, chain disentanglement, anomalous transport of solvent, chain reptation, and external mass transfer limitations. In addition, various experimental techniques have been utilized to characterize polymer dissolution behavior and establish a number of physical phenomena and molecular properties of solvent and polymer. Some of these techniques are differential refractometry, optical microscopy, fluorescence, gravimetry, interferometry, NMR, and FT-IR imaging. While the research on polymer dissolution is vast, extended understanding of polymer dissolution is necessary to facilitate the ever rapid changing technology for which polymer dissolution is applicable.

## References

[1] Kufner M, Kufner S. Micro-optics and lithography. Brussels: VUBPRESS; 1997.

[2] Narasimhan B, Mallapragada SK. Dissolution of amorphous and semicrystalline polymers: mechanisms and novel applications. Recent Res Dev Macromol Res 1998;3(Part 2):311–24.

[3] Tsay CS, McHugh AJ. Mass transfer modeling of asymmetric membrane formation by phase inversion. J Polym Sci 1990; 28(8):1327–65.

[4] Yilmaz L, McHugh AJ. Modeling of asymmetric membrane formation. II. The effects of surface boundary conditions. J Appl Polym Sci 1988;35(7):1967–79.

[5] Kesting RE, Fritzsche AK. Polymeric gas separation membranes. New York, NY: Wiley; 1993.

[6] Nauman EB, Lynch JC. US Patent 5 198 471; 1993.

[7] Nauman EB, Lynch JC. US Patent 5 278 282; 1994.

[8] Srivastava AP, Nauman BE. Kinetics of solvent induced melting of semicrystalline polymers. Polym Mater Sci Engng Proc 1993;69:307–8.

[9] Lee PI, Good WR, editors. Controlled-release technology pharmaceutical applications. Washington, DC: American Chemical Society; 1987.

[10] Langer R, Vacanti JP. Artifical organs. Sci Am 1995;273(3): 130–3.

[11] Peppas NA, Langer R. New challenges in biomaterials. Science 1994;263(5154):1715–20.

[12] Ueberreiter K. The solution process. In: Crank J, Park GS, editors. Diffusion in polymers. New York, NY: Academic Press; 1968. p. 219–57.

[13] Asmussen R, Raptis G, Diplomarbeit FU. Berlin; 1965.

[14] Asmussen F, Ueberreiter K. Velocity of dissolution of polymers. Part II. J Polym Sci 1962;57(165):199–208.

[15] Krasicky PD, Groele RJ, Jubinsky JA, Rogdriguez F. Studies of dissolution phenomena in microlithography. Polym Engng Sci 1987;27(4):282–5.

[16] Krasicky PD, Groele RJ, Rodriguez F. Measuring and modeling the transition layer during the dissolution of glassy polymer films. J Appl Polym Sci 1988;35(3):641–51.

[17] Pekcan Ö, Canpolat M, Kaya D. In situ fluorescence experiments for real-time monitoring of annealed high-T latex film dissolution. J Appl Polym Sci 1996;60(12): 2105–12.

[18] Cooper WJ, Krasicky PD, Rodriguez F. Effects of molecular weight and plasticization on dissolution rates of thin polymer films. Polymer 1985;26(7):1069–72.

[19] Manjkow J, Papanu JS, Hess DW, Soane (Soong) DS, Bell AT. Influence of processing and molecular parameters on

the dissolution rate of poly-(methyl methacrylate) thin films. J Electrochem Soc 1987;134(8):2003–7.

[20] Papanu JS, Hess DW, Bell AT, Soane DS. Dissolution of thin poly(methyl methacrylate) films in ketones, binary ketone/alcohol mixtures, and hydroxy ketones. J Electrochem Soc 1989;136(10):3077–83.

[21] Papanu JS, Hess DW, Soane (Soong) DS, Bell AT. Swelling of poly(methyl methacrylate) thin films in low molecular weight alcohols. J Appl Polym Sci 1990;39(4):803–23.

[22] Parsonage EE, Peppas NA, Lee PI. Properties of positive resists. II. Dissolution characteristics of irradiated poly (methyl methacrylate) and poly(methyl methacrylate-*co*-maleic anhydride). J Vac Sci Technol 1987;B5(2):538–45.

[23] Pekcan Ö, Uǧur S, Yilmaz Y. Real-time monitoring of swelling and dissolution of poly(methyl methacrylate) discs using fluorescence probes. Polymer 1997;38(9):2183–9.

[24] Pekcan Ö, Uǧur S. Molecular weight effect on polymer dissolution: a steady state fluorescence study. Polymer 2002;43(6):1937–41.

[25] Ouano AC, Carothers FA. Dissolution dynamics of some polymers: solvent–polymer boundaries. Polym Engng Sci 1980;20(2):160–6.

[26] Gipstein E, Ouano AC, Johnson DE, Need III OU. Parameters affecting the sensitivity of poly(methyl methacrylate) as a positive lithographic resist. Polym Engng Sci 1977;17(6):396–401.

[27] Groele RJ, Rodriguez F. Dissolution rates of polymers and copolymers based on methyl, ethyl, and butyl methacrylate. J Coat Technol 1989;61(774):55–8.

[28] Reinhardt M, Pfeiffer K, Lorkowski H-J. Polymer dissolution. 1. On the dissolution behavior of copolymers of methyl methacrylate and methacrylic acid. J Appl Polym Sci 1994;51(2):297–301.

[29] Ouano AC. Dissolution kinetics of polymers: effect of residual solvent content. In: Seymour R, Stahl GA, editors. Macromolecular solutions: solvent–property relationships in polymers. New York, NY: Permagon Press; 1982.

[30] Cooper WJ, Krasicky PD, Rodriguez FJ. Dissolution rates of poly(methyl methacrylate) films in mixed solvents. Appl Polym Sci 1986;31(1):65–73.

[31] Manjkow J, Papanu JS, Soong DS, Hess SW, Bell AT. An in situ study of dissolution and swelling behavior of poly-(methyl methacrylate) thin films in solvent/nonsolvent binary mixtures. J Appl Phys 1987;62(2):682–8.

[32] Mao S-Z, Feng H-Q. Study of the dissolution process of polystyrene in concentrated cyclohexane solution by NMR relaxation. Colloid Polym Sci 1998;276(3):247–51.

[33] Rodriguez F, Krasicky PD, Groele RJ. Dissolution rate measurements. Solid State Technol 1985;28(5):125–31.

[34] Harland RS, Gazzaniga A, Sangani ME, Colombo P, Peppas NA. Drug–polymer matrix swelling and dissolution. Pharmaceut Res 1988;5(8):488–94.

[35] Rao V, Hinsberg WD, Frank CW, Pease RFW. The influence of sensitizer spatial distribution on the dissolution mechanism of diazonaphthoquinone resists. Proc. SPIE 1992;1672(Adv Resist Technol Process IX):214–30.

[36] Parsonage EE, Peppas NA. Properties of positive resists. 1. Irradiation-induced degradation and sensitivity of certain methyl methacrylate copolymers. Br Polym J 1987;19(5):469–77.

[37] Drummond R, Boydston GL, Peppas NA. Properties of positive resists. III. The dissolution behavior of poly(methyl methacrylate-*co*-maleic anhydride). J Appl Polym Sci 1990;39(11/12):2267–77.

[38] Hansen CM. Hanson solubility parameters: a user's handbook. Boca Raton, FL: CRC Press; 2000.

[39] Grulke EA. Solubility parameter values. In: Brandrup J, Immergut EH, Grulke EA,, editors, 4th ed. Polymer handbook, vol. 7. New York, NY: Wiley; 1999. p. 675–714.

[40] Bicerano J. Prediction of polymer properties, 1st ed. New York, NY: Marcel Dekker; 1993.

[41] Sanchez IC. Statistical thermodynamics of polymer blends. In: Paul DR, Newman S, editors. Polymer blends. New York, NY: Academic Press; 1978. p. 115–39.

[42] Kaelble DH. Computer aided design of polymers and composites. New York, NY: Marcel Dekker; 1985.

[43] Fedors RF. A method for estimating both the solubility parameters and molar volumes of liquids. Polym Engng Sci 1974;14(2):147–54.

[44] Hwang S-T, Kammermeyer K. Membranes in separations. Malabar: Robert E. Krieger Publishing Company; 1984.

[45] Sears JK, Darby JR. The technology of plasticizers. New York, NY: Wiley; 1982.

[46] Gardon JL. Relationship between cohesive energy densities of polymers and Zisman's critical surface tensions. J Phys Chem 1963;67(9):1935–6.

[47] Girifalco LA, Good RJ. A theory for the estimation of surface and interfacial energies. I. Derivation and application to interfacial tension. J Phys Chem 1957;61(6):904–9.

[48] Good RJ. Estimation of surface and interfacial energies. VI. Surface energies of some fluorocarbon surfaces from contact angle measurements. Adv Chem Ser 1964;43:74–87.

[49] Lee LH. Relationships between surface wettability and glass temperatures of high polymers. J Appl Polym Sci 1968;12(4):719–30.

[50] Hildebrand JH, Scott RL. The solubility of nonelectrolytes, 3rd ed. New York, NY: Dover Publications; 1964.

[51] Gardon JL. Variables and interpretation of some destructive cohesion and adhesion tests. In: Patrick RL, editor. Treatise on adhesion and adhesives. New York, NY: Marcel Dekker; 1967.

[52] Hayes RA. The relationship between glass temperature, molar cohesion, and polymer structure. J Appl Polym Sci 1961;5(15):318–21.

[53] Hildebrand JH. Study of the action of alkali on certain zinc salts by means of the hydrogen electrode. J Am Chem Soc 1916;38(4):785–8.

[54] Scatchard G. Equilibria in nonelectrolyte solutions in relation to the vapor pressures and densities of the components. Chem Rev 1931;8(2):321–33.

[55] Scatchard G. Equilibrium in nonelectrolyte mixtures. Chem Rev 1949;44(1):7–35.

[56] Burrel H. Official Digest 1955;27:726.

[57] Beerbower A. Environmental capability of liquid lubricants. In: Interdisciplinary approach to liquid lubricant technology. NASA Publication SP-318; 1973. p. 365–431.

[58] Watson KM. Prediction of critical temperatures and heats of vaporization. Ind Engng Chem 1931;23:360–4.

[59] Watson KM. Thermodynamics of the liquid state. Generalized prediction of properties. Ind Engng Chem 1943;35: 398–406.

[60] Blanks RF, Prausnitz JM. Thermodynamics of polymer solubility in polar and nonpolar systems. Ind Engng Chem Fundam 1964;3(1):1–8.

[61] Hansen CM. Solubility parameters. In: Koleske JV, editor. Paint testing manual, manual 17. Philadelphia, PA: American Society for Testing and Materials; 1995. p. 383–404.

[62] Hansen CM, Skaarup K. III. Independent calculation of the parameter components. J Paint Technol 1967;39(511): 511–4.

[63] Hansen CM, Beerbower A. Solubility parameters. In: Standen A, editor. Kirk–Othmer encyclopedia of chemical technology, 3rd ed. New York, NY: Wiley; 1971. p. 889–910.

[64] Dunkel MZ. Calculation of intermolecular forces in organic compounds. Phys Chem 1928;138:42–54.

[65] Small PA. Some factors affecting the solubility of polymers. J Appl Chem 1953;3:71–80.

[66] Rheineck AE, Lin KF. Solubility parameter calculations based on group contributions. J Paint Technol 1968;40(527): 611–6.

[67] Hoy KL. New values of the solubility parameters from vapor pressure data. J Paint Technol 1970;42(541):76–118.

[68] Haggenmacher JE. The heat of vaporization as a function of pressure and temperature. J Am Chem Soc 1946;68(8): 1633–4.

[69] Van Krevelen DW, Hoftzyer PJ. Properties of polymers: their correlation with chemical structure; their numerical estimation and prediction from additive group contributions, 3rd ed. Amsterdam: Elsevier; 1990.

[70] Van Krevelen DW. Chemical structure and properties of coal. XXVIII. Coal constitution and solvent extraction. Fuel 1965;44(4):229–42.

[71] Painter P, Coleman M. Fundamentals of polymer science, 2nd ed. Lancaster, PA: Technomic Publishing Co; 1997.

[72] Burke J. AIC Book and Paper Group Annual 1984;3:13.

[73] Crowley JD, Teague Jr GS, Lowe Jr JW. A three-dimensional approach to solubility. J Paint Technol 1966;38(496): 269–80.

[74] Crowley JD, Teague Jr GS, Lowe Jr JW. A three-dimensional approach to solubility. II. J Paint Technol 1967;39(504): 19–27.

[75] Hansen CM. 14th International Conference on Coating. Copenhagen: Community and Care; 1994.

[76] Prigogine I. The molecular theory of solutions. Amsterdam: North-Holland; 1957. with collaboration of Bellemans A, Mathot A.

[77] Hansen CM, Just L. Prediction of environmental stress cracking in plastics with Hansen solubility parameters. Ind Engng Chem Res 2001;40(1):21–5.

[78] Teas JP. Graphic analysis of resin solubilities. J Paint Tech 1968;40(516):19–25.

[79] Barton AFM. Handbook of solubility parameters and other cohesion parameters. Boca Raton, FL: CRC Press; 1991.

[80] Narasimhan B. Mathematical models describing polymer dissolution: consequences for drug delivery. Adv Drug Deliv Rev 2001;48(2/3):195–210.

[81] Narasimhan B, Peppas NA. The physics of polymer dissolution: modeling approaches and experimental behavior. Adv Polym Sci 1997;128:158–207.

[82] Ribar T. FT-IR imaging of the dissolution of poly(a-methystyrene) in solvent mixtures and spectroscopic analysis of vapor diffusion through an aniline oligomer chemical sensor. Master's Thesis, Case Western Reserve Univeristy, 2001.

[83] Tu Y-O, Ouano AC. Model for the kinematics of polymer dissolution. IBM J Res Develop 1977;21(2):131–42.

[84] Devotta I, Ambeskar VD, Mandhare AB, Mashelkar RA. The life time of a dissolving polymeric particle. Chem Engng Sci 1994;49(5):645–54.

[85] Ranade VV, Mashelkar RA. Convective diffusion from a dissolving polymeric particle. AIChE J 1995;41(3):666–76.

[86] Devotta I, Badiger MV, Rajamohanan PR, Ganapathy S, Mashelkar RA. Unusual retardation and enhancement in polymer dissolution: role of disengagement dynamics. Chem Engng Sci 1995;50(16):2557–69.

[87] Zielinski JM, Duda JL. Predicting polymer/solvent diffusion coefficients using free-volume theory. AIChE J 1992;38(3): 405–15.

[88] Devotta I, Mashelkar RA. Role of thermodynamic and kinetic factors in polymer dissolution in mixed solvents. Chem Engng Commun 1996;156:31–45.

[89] Papanu JS, Soane (Soong) DS, Bell AT, Hess DW. Transport models for swelling and dissolution of thin polymer films. J Appl Polym Sci 1989;38(5):859–85.

[90] Siepmann J, Göpferich A. Mathematical modeling of bioerodible, polymeric drug delivery systems. Adv Drug Deliv Rev 2001;48(2/3):229–47.

[91] Siepmann J, Kranz H, Bodmeier R, Peppas NA. HPMC-matrices for controlled drug delivery: a new model combining diffusion, swelling, and dissolution mechanisms and predicting the release kinetics. Pharm Res 1999;16(11): 1748–56.

[92] Siepmann J, Paeratakul O, Bodmeier R. Modeling plasticizer uptake in aqueous polymer dispersions. Int J Pharm 1998; 165(2):191–200.

[93] Narasimhan B, Peppas NA. Molecular analysis of drug delivery systems controlled by dissolution of the polymer carrier. J Pharm Sci 1997;86(3):297–304.

[94] Lee PI, Peppas NA. Prediction of polymer dissolution in swellable controlled-release systems. J Contr Rel 1987;6: 207–15.

[95] Lee H-R, Lee Y-D. Mathematical models and experiments for swelling phenomena before dissolution of polymer films. Chem Engng Sci 1991;46(7):1771–9.

[96] Brochard F, de Gennes PG. Kinetics of polymer dissolution. Phys Chem Hydrodynam 1983;4(4):313–22.

[97] Herman MF, Edwards SF. A repetition model for polymer dissolution. Macromolecules 1990;23(15):3662–71.

[98] de Gennes PG. Scaling concepts in polymer physics. Ithaca, NY: Cornell University Press; 1979.

[99] Peppas NA, Wu JC, von Meerwal ED. Mathematical modeling and experimental characterization of polymer dissolution. Macromolecules 1994;27(20):5626–38.

[100] de Gennes PG, Leger L. Dynamics of entangled polymer chains. Annu Rev Phys Chem 1982;33:49–61.

[101] de Gennes PG. Repetition of a polymer chain in the presence of fixed obstacles. J Chem Phys 1971;55(2):572–9.

[102] Edwards SF. Statistical mechanics of polymerized material. Proc Phys Soc 1967;92(1):9–16.

[103] Wu JC, Peppas NA. Numerical simulation of anomalous penetrant diffusion in polymers. Appl Polym Sci 1993; 49(10):1845–56.

[104] Vrentas JS, Vrentas CM. Dissolution of rubbery and glassy polymers. J Polym Sci, B, Polym Phys 1998;36(14): 2607–14.

[105] Narasimhan B, Peppas NA. Disentanglement and repetition during the dissolution of rubbery polymers. J Polym Sci, B, Polym Phys 1996;34(5):947–61.

[106] Narasimhan B, Peppas NA. On the importance of chain repetition in models of dissolution of glassy polymers. Macromolecules 1996;29(9):3283–91.

[107] Conte U, Colombo P, Gazzaniga A, Sangalli ME, La Manna A. Swelling-activated drug delivery systems. Biomaterials 1988;9(6):489–93.

[108] Ju RTC, Nixon PR, Patel MV. Drug release from hydrophilic matrices. 1. New scaling laws for predicting polymer and drug release based on the polymer disentanglement concentration and the diffusion layer. J Pharm Sci 1995;84(12): 1455–63.

[109] Ju RTC, Nixon PR, Patel MV, Tong DM. Drug release from hydrophilic matrices. 2. A mathematical model based on the polymer disentanglement concentration and the diffusion layer. J Pharm Sci 1995;84(12):1464–77.

[110] Ju RTC, Nixon PR, Patel MV. Diffusion coefficients of polymer chains in the diffusion layer adjacent to a swollen hydrophilic matrix. J Pharm Sci 1997;86(11):1293–8.

[111] Doi M, Edwards SF. The theory of polymer dynamics, 2nd ed. Oxford: Clarendon Press; 1986.

[112] Papanu JS, Hess DW, Bell AT, Soane DS. In situ ellipsometry to monitor swelling and dissolution of thin polymer films. J Electrochem Soc 1989;136(4):1195–200.

[113] McCrackin FL. Natl Bur Std, Tech Note 1969;479.

[114] Limm W, Stanton D, Dimnik GP, Winnik MA. Solvent penetration and photoresist dissolution: a fluorescence quenching and interferometry study. J Appl Polym Sci 1988;35(8):2099–116.

[115] Uğur S, Pekcan ÖJ. Fluorescence technique to study thickness effect on dissolution of latex films. J Appl Polym Sci 2000;77(5):1087–95.

[116] Rao V, Hinsberg WD, Frank CW, Pease RFW. Langmuier–Blodgett deposition to evaluate dissolution behavior of multicomponent resists. In: Thompson LF, Willson CG, Tagawa S, editors. Polymers for microelectronics resists and dielectrics. Washington, DC: American Chemical Society; 1994. p. 220–34.

[117] Devotta I, Premnath V, Badiger MV, Rajamohanan PR, Ganapathy S, Mashelkar RA. On the dynamics of mobilization in swelling-dissolving polymeric systems. Macromolecules 1994;27(2):532–9.

[118] Weisenberger LA, Koenig JL. NMR imaging of solvent diffusion in polymers. Appl Spectrosc 1989;43(7):1117–26.

[119] Hyde TM, Gladden LF, Mackley MR, Gao P. Quantitative nuclear magnetic resonance imaging of liquids in swelling polymers. J Polym Sci, A, Polym Chem 1995;33(11): 1795–806.

[120] Koenig J. FTIR imaging of polymer dissolution. Adv Mater 2002;14(6):457–60.

[121] Ribar T, Bhargava R, Koenig JL. FT-IR imaging of polymer dissolution by solvent mixtures. 1. Solvents. Macromolecules 2000;33(23):8842–9.

[122] Ribar T, Koenig JL. FTIR imaging of polymer dissolution. 2. Solvent/nonsolvent mixtures. Macromolecfsules 2001; 34(23):8340–6.

[123] Miller-Chou BA, Koenig JL. FT-IR imaging of polymer dissolution by solvent mixtures. 3. Entangled polymer chains with solvents. Macromolecules 2002;35(2):440–4.

[124] Miller-Chou BA, Koenig JL. Submitted for publication.

[125] Miller-Chou BA, Koenig JL. Submitted for publication.

[126] Miller-Chou BA, Koenig JL. Submitted for publication.

[127] Rafferty DW, Koenig JL. Submitted for publication.

[128] Rafferty DW, Koenig JL. FTIR imaging for the characterization of controlled-release drug delivery applications. J Contr Rel 2002;83(1):29–39.

[129] Gonzales-Benito J, Koenig JL. FTIR imaging of the dissolution of polymers. 4. Poly(methyl methacrylate) using a cosolvent mixture (carbon tetrachloride/methanol). Macromolecules 2002;35(14):7361–7.